



Since January 2020 Elsevier has created a COVID-19 resource centre with free information in English and Mandarin on the novel coronavirus COVID-19. The COVID-19 resource centre is hosted on Elsevier Connect, the company's public news and information website.

Elsevier hereby grants permission to make all its COVID-19-related research that is available on the COVID-19 resource centre - including this research content - immediately available in PubMed Central and other publicly funded repositories, such as the WHO COVID database with rights for unrestricted research re-use and analyses in any form or by any means with acknowledgement of the original source. These permissions are granted for free by Elsevier for as long as the COVID-19 resource centre remains active.



Dual targeting of cytokine storm and viral replication in COVID-19 by plant-derived steroidal pregnanes: An *in silico* perspective

Gideon A. Gyebi^{a,*}, Oludare M. Ogunyemi^b, Ibrahim M. Ibrahim^c, Saheed O. Afolabi^d, Joseph O. Adebayo^e

^a Department of Biochemistry, Faculty of Science and Technology Bingham University, Karu, Nasarawa, Nigeria

^b Human Nutraceuticals and Bioinformatics Research Unit, Department of Biochemistry, Salem University, Lokoja, Nigeria

^c Department of Biophysics, Faculty of Sciences, Cairo University, Giza, Egypt

^d Department of Pharmacology and Therapeutics, Faculty of Basic Medical Sciences University of Ilorin, Ilorin, Nigeria

^e Department of Biochemistry, Faculty of Life Sciences, University of Ilorin, Ilorin, Nigeria

ARTICLE INFO

Keywords:

COVID-19

Cytokine storm

Glucocorticoid receptors

Pregnanes

Anti-inflammatory activity

Antiviral activity

ABSTRACT

The high morbidity and mortality rate of Severe Acute Respiratory Syndrome CoronaVirus 2 (SARS-CoV-2) infection arises majorly from the Acute Respiratory Distress Syndrome and “cytokine storm” syndrome, which is sustained by an aberrant systemic inflammatory response and elevated pro-inflammatory cytokines. Thus, phytocompounds with broad-spectrum anti-inflammatory activity that target multiple SARS-CoV-2 proteins will enhance the development of effective drugs against the disease. In this study, an in-house library of 117 steroidal plant-derived pregnanes (PDPs) was docked in the active regions of *human* glucocorticoid receptors (*hGRs*) in a comparative molecular docking analysis. Based on the minimal binding energy and a comparative dexamethasone binding mode analysis, a list of top twenty ranked PDPs docked in the agonist conformation of *hGR*, with binding energies ranging between -9.8 and -11.2 kcal/mol, was obtained and analyzed for possible interactions with the *human* Janus kinases 1 and Interleukins-6 and SARS-CoV-2 3-chymotrypsin-like protease, Papain-like protease and RNA-dependent RNA polymerase. For each target protein, the top three ranked PDPs were selected. Eight PDPs (bregenin, hirundigenin, anhydroholantogenin, atratogenin A, atratogenin B, glaucogenin A, glaucogenin C and glaucogenin D) with high binding tendencies to the catalytic residues of multiple targets were identified. A high degree of structural stability was observed from the 100 ns molecular dynamics simulation analyses of glaucogenin C and hirundigenin complexes of *hGR*. The selected top-eight ranked PDPs demonstrated high druggable potentials and favourable *in silico* ADMET properties. Thus, the therapeutic potentials of glaucogenin C and hirundigenin can be explored for further *in vitro* and *in vivo* studies.

1. Introduction

Coronavirus disease 2019 (COVID-19) is a clinical syndrome, caused by Severe Acute Respiratory Syndrome Corona Virus 2 (SARS-CoV-2) [1]. The clinical presentation of SARS-CoV-2 infections ranges from asymptomatic condition or mild symptoms (such as fever, cough, and generalized malaise) in the majority of the cases to severe respiratory failure. The early stage of infection, progresses to interstitial pneumonia and acute respiratory distress syndrome (ARDS) in nearly 10–20% of the cases, especially in the elderly and people with co-morbidities [2]. The pathophysiology of SARS-CoV-2 infection is a complex mechanism that is known to mobilize several biomolecules of the immune and

hematologic systems [3].

Cytokines are a group of polypeptide signaling molecules responsible for regulating a large number of biological processes via cell surface receptors [4]. The term “cytokine storm”, a condition characterized by an exaggerated activation of the immune system was first associated with onset of the graft-versus-host disease [5] and later known to be involved in several viral infections [6]. The exaggerated cytokine release in response to viral infection, has emerged as one of the mechanisms leading to acute respiratory distress syndrome and multiple-organ failure in COVID-19 [7]. In this regard, recent studies have shown that patients with COVID-19 have higher levels of inflammatory cytokines, such as interleukin (IL)-1 β , IL-2, IL-6, IL-7, IL-8, IL-9, IL-10, IL-18, tumor necrosis factor (TNF)- α , granulocyte colony-stimulating factor (G-CSF),

* Corresponding author. Department of Biochemistry, Faculty of Science and Technology, P.M.B 005, Karu, Nasarawa State, Nigeria.

E-mail addresses: gyebi.gideon@binghamuni.edu.ng, gideonagyebi@gmail.com (G.A. Gyebi).

Abbreviations

COVID-19	The Coronavirus disease 2019
SARS-CoV-2	Severe Acute Respiratory Syndrome Corona Virus 2
sRdRp	SARS-CoV-2 RNA-dependent RNA polymerase
GR	Glucocorticoid receptors
hGRag	Human glucocorticoid receptors in agonist conformation
hGRagt	Human glucocorticoid receptors in antagonist conformation
JKs	Janus kinases
3CLpro	3-chymotrypsin-like protease
PLpro	Papain-like protease
ARDS	Acute Respiratory Distress Syndrome
PDPs	Plant derived pregnanes
IL	Interleukins
IFN	Interferons

granulocyte-macrophage colony-stimulating factor, fibroblast growth factor, macrophage inflammatory protein 1, compared to healthy individuals [8]; circulating levels of IL-6, IL-10, and TNF- α also correlated with illness severity as they were significantly higher in intensive care unit (ICU) patients compared to mild/moderate cases. At this point, anti-viral treatment alone is not enough and should be combined with appropriate anti-inflammatory treatment. Anti-rheumatic drugs, which are tried for managing cytokine storm of SARS-CoV-2 infection include: corticosteroids, JAK inhibitors, IL-6 inhibitors, IL-1 inhibitors, anti-TNF- α agents, hydroxychloroquine, intravenous immunoglobulin (IVIG), and colchicines [9].

The interaction of glucocorticoids receptors (GR) and its ligands, glucocorticoids (GCs), have been explored for the modulation of cytokines in acute and chronic inflammatory diseases [10]. Glucocorticoids modulate cytokine expression by several genomic mechanisms. The activated GR complex: (i) binds to the promoter responsive elements, thereby inactivating key pro-inflammatory transcription factors (e.g. AP-1, NF kappa B); (ii) upregulates the expression of cytokine inhibitory proteins, e.g. I kappa B, which inactivates the transcription factor NF kappa B, thereby suppressing the secondary expression of a series of cytokines; and lastly, (iii) reduces the half-lives and utility of cytokine mRNAs [11]. Unfortunately, the use of GCs is limited by unwanted severe side effects, such as osteoporosis, disorders of glucose and lipid metabolism, and hypertension [12]. Therefore, there is an urgent need for the development of natural compounds with higher anti-inflammatory activity compared to standard GCs, alongside antiviral potential and with accompanied no or low toxicity [13,14]. Janus kinases (JAKs) mediate the signaling of numerous cytokines and growth factors involved in the regulation of inflammation, immunity and hematopoiesis [15]. Among the JAK family members, the JAK1 has the broadest cytokine signaling profile, being the only isoform that pairs with the other three JAKs. The pairing of JAK1 with JAK3 regulates the signaling of the gamma common (γ) cytokines. The pairing of JAK1 with JAK2 regulates the signaling of type I interferons (IFN α , IFN β), type II interferon (IFN γ) and the IL-10 family of cytokines [16]. Inhibitors of the JAK-STAT pathway, such as baricitinib and Ruxolitinib, are used for suppressing proinflammatory cytokine production and systemic inflammation. Interleukin-6 (IL-6) is a pleiotropic cytokine. In general, IL-6 inhibitors prevent human IL-6 from binding to IL-6 receptors, thus impeding the formation of immune signaling complexes on cell surfaces [17].

Along with structural proteins, the SARS viral genomes encode non-structural proteins, including 3-chymotrypsin-like protease (3CL^{pro}), papain-like protease (PLpro), helicase and RNA-dependent RNA polymerase (RdRp) which are important target for the development of

therapeutics [18]. The proteolytic processing of the polyproteins is performed by the viral cysteine proteases to yield 16 non-structural proteins; 3CL^{pro} cleaves and modifies the viral polyproteins at 11 sites while PL^{pro} cleaves the first three sites at the N-terminus [4,19]. The RNA-dependent RNA polymerase (RdRp), is a central component of coronaviral replication/transcription machinery that catalyzes RNA-templated dependent formation of phosphodiester bonds between ribonucleotides. In our recent work, we have demonstrated the potential of some natural compounds as inhibitors of these proteins [20–22].

Recently, dexamethasone, a potent synthetic anti-inflammatory glucocorticoid was declared as the world's first treatment proven effective in reducing the risks of death through cytokine storm among severely ill COVID-19 patients based on clinical trial results [23,24]. Through computational and biological comparison, few plant-derived steroidal compounds have been suggested as modulators of inflammation through interactions with GR (Dean et al., 2017; Morsy et al., 2019). Such plant-derived anti-inflammatory steroids like glycyrrhetic acid [25], guggulsterone [26], boswellic acid [27], withaferin A [28] and diosgenin [29] have a common cyclopentanoperhydrophenanthrene steroid ring structure. Pregnanes are naturally occurring C₂₁ steroidal compounds that have been documented with wide range of bioactivities including anti-inflammatory activity [22,30–32]. Due to the present COVID-19 pandemic, there is urgent need for such plant-derived steroids that may possess dual interference with cytokine storm and viral replication/transcriptase complex but with fewer side effects. Thus, the aim of this study was to screen an in-house library of plant-derived steroidal pregnanes for hGR agonist using a comparative molecular docking approach.

2. Materials and methods

2.1. Retrieval of protein structure

The three-dimensional (3D) structure of human glucocorticoid receptors in the agonist conformation (hGRag) (PDB ID: 4UDC), human glucocorticoid receptors in the antagonist conformation (hGRagt) (PDB ID: 1NHZ), human Interleukin-6 (hIL-6) (PDB ID: 1ALU), human Janus kinase 1 (hJAK1) (PDB ID: 6BBU), SARS-CoV-2 3-chymotrypsin-like protease (s3CL^{pro}) (PDB ID: 6Y84), SARS-CoV-2 papain-like protease (sPL^{pro}) (PDB ID: 6W9C) and SARS-CoV-2 RNA-dependent RNA polymerase (sRdRp) (PDB ID: 6M71) were retrieved from the Protein Data Bank (<http://www.rcsb.org>).

2.2. Protein preparation

The crystal structures of the proteins were processed by removing existing ligands and water molecules while missing hydrogen atoms were added according to the amino acid protonation state at pH 7.0 utilizing Autodock version 4.2 program (Scripps Research Institute, La Jolla, CA). Thereafter, non-polar hydrogens were merged while polar hydrogens were added to each protein. The process was repeated for each protein and subsequently saved into a dockable pdbqt format for molecular docking.

2.3. Ligand preparation

PDPs (117) were compiled from literature search. The Structure Data Format (SDF) structures of the reference compounds: dexamethasone (Dex), mifepristone, methotrexate, ruxolitinib, ritonavir, disulfiram, remdesivir and some of the compounds were retrieved from the PubChem database (www.pubchem.ncbi.nlm.nih.gov); other compounds not present on the database were drawn with Chemdraw version 19. All the compounds and reference compounds were converted to mol2 chemical format using Open babel (O'Boyle et al., 2011). The non-polar hydrogen atoms were merged with the carbons, polar hydrogen charges of the Gasteiger-type were assigned and the internal degrees of freedom

Table 1
Binding site coordinates of human GRs.

	hGRs (Å)	center_x	center_y	center_z	Size_x	Size_y	Size_z
a	hGRag (4UDC)	1.4	41.6	16.9	27.3	21.6	25.9
	hGRagt (1NHZ)	-2.75	15.9	3.25	14.51	33.34	22.24
b	hIL-6 (1ALU)	-8.8	-14.5	4.7	24.4	22.2	17.9
	hJAK1 (6BBU)	12.0	12.0	-15.4	15.4	19.0	27.3
	s3CLpro (6Y84)	9.4	19.2	19.2	19.2	16.0	18.9
	sPLpro (6W9C)	19.5	28.0	18.3	26.8	26.8	34.7
	sRdRp (6M71)	114.6	116.0	123.7	17.0	22.4	25.7

Human glucocorticoid receptors in the agonist conformation (hGRag), human glucocorticoid receptors in the antagonist conformation (hGRagt), human Interleukin-6 (hIL-6) human Janus kinase 1(hJAK1), SARS-CoV-2 3-chymotrypsin-like protease (s3CL^{pro}), SARS-CoV-2 papain-like protease (sPL^{pro}) and SARS-CoV-2 RNA-dependent RNA polymerase (sRdRp).

and torsions were set to zero. The protein and ligand molecules were further converted to the dockable pdbqt format using Autodock tools.

2.4. Molecular docking study

2.4.1. Competitive molecular docking to the human GRs

A competitive molecular docking approach [33,34] was employed for a structure based identification of agonist of the hGR protein. The approach combined separate molecular docking models for hGR in the agonist and antagonist conformations. True agonists and antagonists that were native ligands to the co-crystallized structures were extracted and first used to evaluate the ability of this approach to differentiate agonists and antagonists. An initial docking analysis of the PDPs (117) and reference compounds (positive control: dexamethasone and negative control: mifepristone) to the hGRag (4UDC) was conducted. Ranking based on minimum binding energies and interactions with catalytic residues was employed to generate a list of the top twenty PDPs hits with the highest binding tendencies. (Table S1). A competitive docking analysis of the top twenty PDPs to another hGRagt (1NHZ) in the antagonist conformation (reference compounds: mifepristone as positive control and dexamethasone as negative control) was further conducted. Both hGRag and hGRagt were co-crystallized with dexamethasone and mifepristone (the positive controls) respectively. The

PDPs, reference compounds and the hGR proteins were loaded into PyRx (Python prescription) 0.8 [35] with the incorporation of Autodock vina [36]. For each of the docking steps, the ligands were imported via the OpenBabel [37], a plug-in tool in PyRx 0.8. The Universal Force Field (UFF) was used as the energy minimization parameter and conjugate gradient descent as the optimization algorithm. The binding site coordinates of the active site regions of the hGRag as defined by the grid boxes were used for docking analysis (Table 1a). All the other parameters were kept as default. After the completion of the docking process, the binding affinities of the protein for the compounds for the selected clusters were recorded. The compounds were then ranked by their binding energies.

2.4.2. Active site targeted molecular docking to other proteins targets

Using the same protocol above, the top twenty PDPs with the lowest binding energies to the hGRag in the agonist conformation and the reference inhibitors were docked to the active region of five proteins: human interleukin-6, human janus kinases, SARS-CoV-2 3-chymotrypsin-like protease, SARS-CoV-2 papain-like protease and SARS-CoV-2 RNA-dependent RNA polymerase as defined by the grid boxes (Table 1b). The molecular interactions of the top three PDPs with the highest binding affinities to each of the proteins and the reference compounds were viewed with Discovery Studio Visualizer version 16.

2.5. Molecular dynamics simulation

Molecular Dynamics Simulation (MDS) was performed on the hGR in the agonist conformation (apo protein), Dex and top-two PDPs complexed with hGRag protein using NAMD software version 2.13 [38]. Necessary files for MDS were generated using CHARMM-GUI webserver [39,40]. For each complex or apo protein, the system was minimized for 10,000 steps in constant number of atoms, constant volume and constant temperature (NVT) ensemble then a production run for 100 ns in NVT ensemble was performed. Temperature was set to be 310 K and salt concentration was set to be the physiological concentration 0.154 M NaCl. Afterwards, calculations of Backbone-Root Mean Square Deviation (RMSD), Per residue Root Mean Square Fluctuations (RMSF), Radius of Gyration (RoG), Surface Accessible Surface Area (SASA) were performed using VMD TK console scripts [41].

2.5.1. Binding free energy calculations

Molecular Mechanics – Generalized Born Surface Area (MM-GBSA) implemented in Amertools 17 is utilized to calculate the binding free energy in Dex and the top two-ranked pregnanes complexed with hGRag

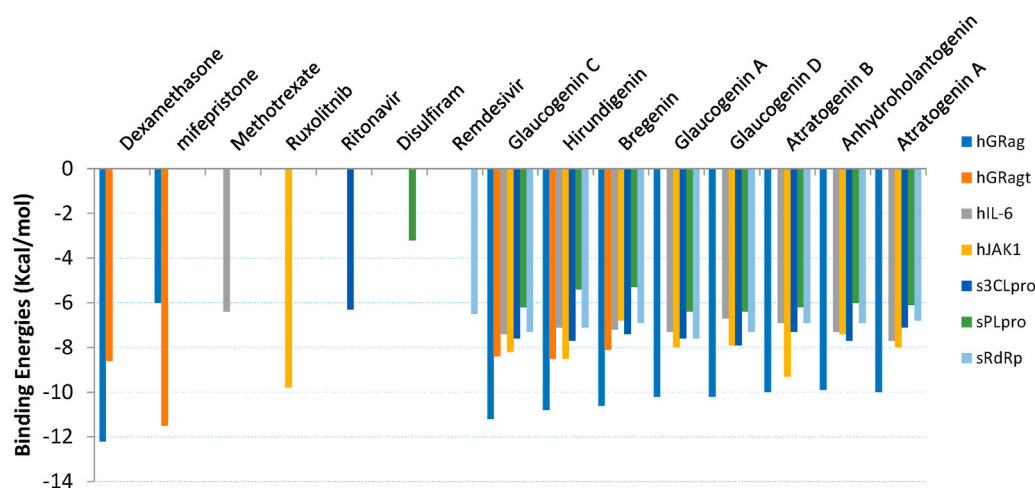


Fig. 1. Binding energies of plant-derived pregnanes for selected protein targets in SARS-COV-2 and human: Human glucocorticoid receptors in the agonist conformation (hGRag); human Interleukin-6 (hIL-6), human Janus kinases (hJAK1); SARS-CoV-2 3-chymotrypsin-like protease (s3CL^{pro}); SARS-CoV-2 papain-like protease (sPL^{pro}) and SARS-CoV-2 RNA-dependent RNA polymerase (sRdRp).

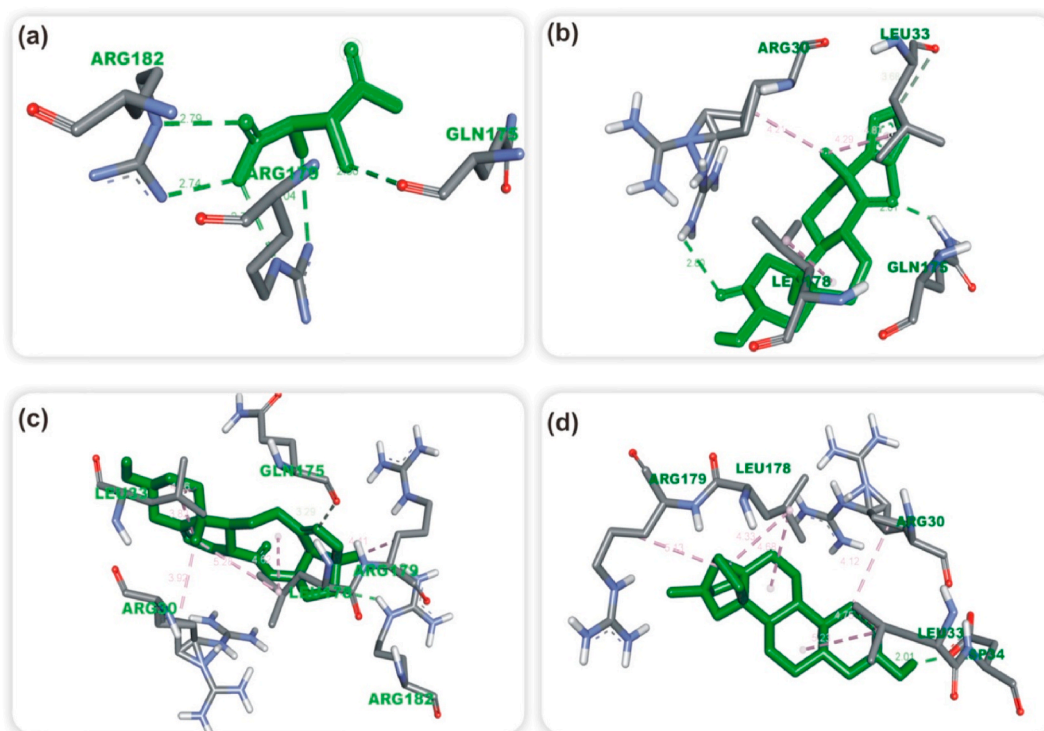


Fig. 3. Amino acid interactions of pregnanes in binding cavity of human Interleukin-6. Stick representation of ligands are coloured green while interacting amino acids are in grey colour (a) L(+)-tartaric(reference inhibitor) (b) atratogenin A (c) glaucogenin C (d) anhydroholantogenin. Types of interactions are represented by green-dotted lines: H-bonds; light purple-dotted line: hydrophobic interactions (Pi-Alkyl, Alkyl & pi-stacking); purple-dotted line: Pi-Pi T Shaped; yellow-dotted lines: Pi-sulphur interactions, pi-stacking interactions. Three-letter abbreviations of amino acids are in black colour.

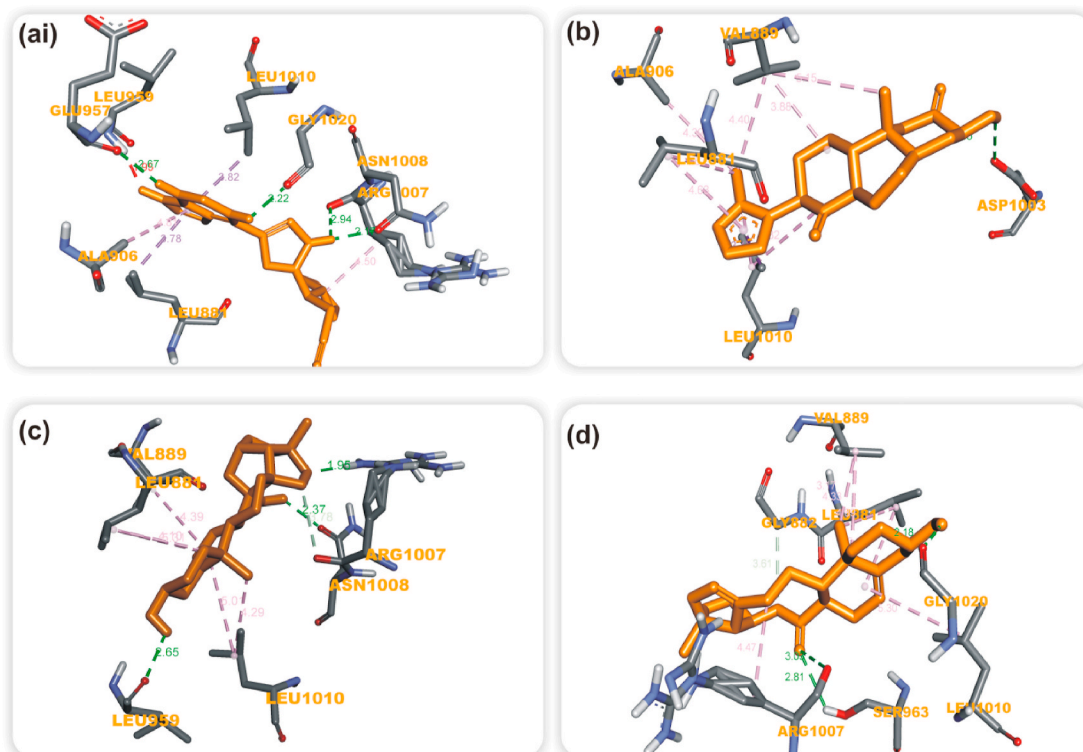


Fig. 4. Amino acid interactions of pregnanes in binding cavity of human Janus kinase 1. Stick representations of ligands are coloured orange while interacting amino acids are in grey colour (a) ruxolitinib (reference inhibitor) (b) atratogenin B (c) hirundigenin (c) glaucogenin C. Types of interactions are represented by green-dotted lines: H-bonds; light purple-dotted line: hydrophobic interactions (Pi-Alkyl, Alkyl & pi-stacking); purple-dotted line: Pi-Pi T Shaped; yellow-dotted lines: Pi-sulphur interactions, pi-stacking interactions. Three-letter abbreviations of amino acids are in black colour.

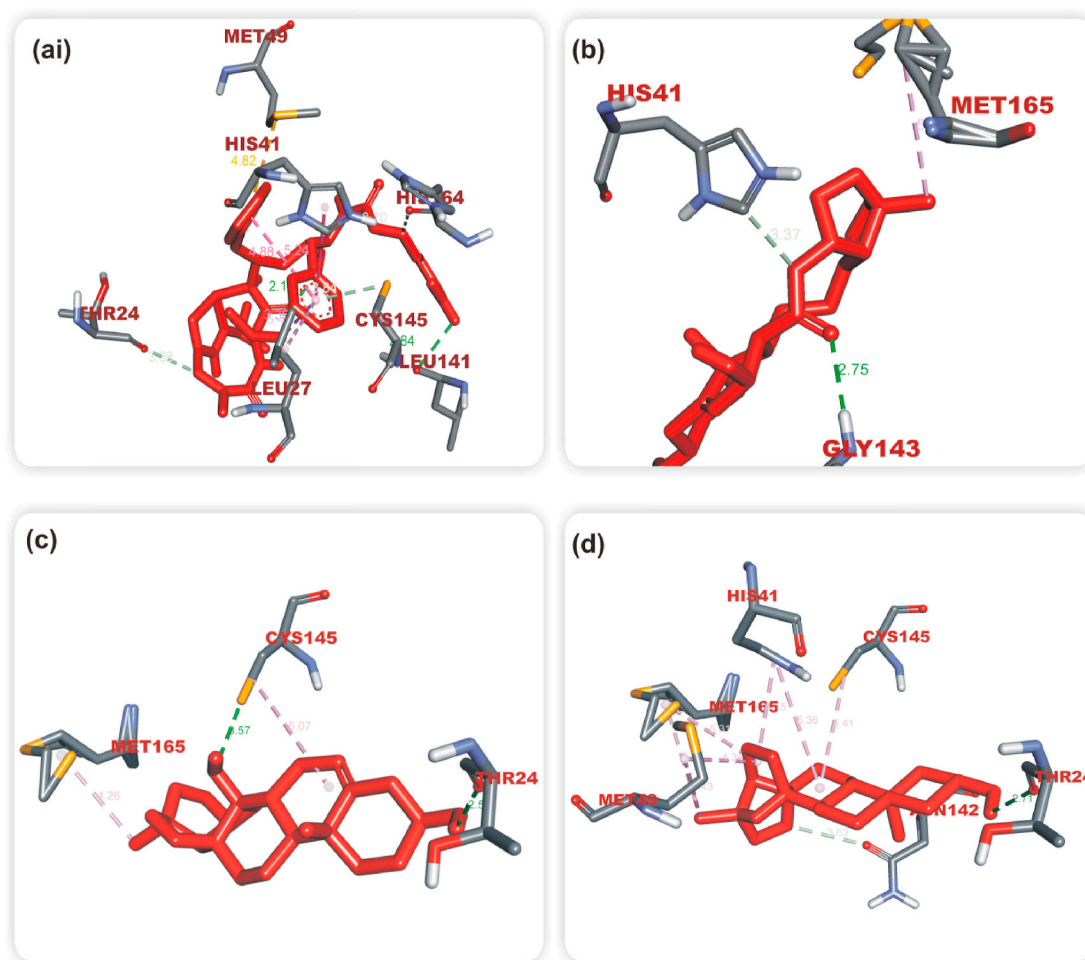


Fig. 5. Amino acid interactions of pregnanes in binding cavity of 3-chymotrypsin-like protease of SARS-CoV-2. Stick representations of ligands are coloured red while interacting amino acids are in grey colour (a) Ritonavir (reference inhibitor) (b) glaucogenin D (c) hirundigenin (c) anhydroholantogenin. Types of interactions are represented by green-dotted lines: H-bonds; light purple-dotted line: hydrophobic interactions (Pi-Alkyl, Alkyl & pi-stacking); purple-dotted line: Pi-Pi T Shaped; yellow-dotted lines: Pi-sulphur interactions, pi-stacking interactions. Three-letter abbreviations of amino acids are in black colour.

three ranked PDPs that demonstrated the highest binding tendencies are represented in Figs. 2–7. The interacting residues of the proteins with respective ligand groups were majorly through H-bond, hydrophobic interactions and few other bonds (Table 2). The revalidation of the docking pattern of the native ligand (dexamethasone) co-crystallized with *hGRag* showed that dexamethasone was docked into to ligand-binding domain (LBD) of *hGRag*. The A-ring of dexamethasone was positioned adjacent to the β -strands 1 and 2 while the D ring was close to helix 12 of *hGRag*. The 3'-carbonyl oxygen of the A ring formed a hydrogen bond to the guanidinium group of ARG⁶¹¹ of *hGRag*. On the C ring, the 11 α -hydroxyl group formed a hydrogen bond with the carbonyl group of LEU⁵⁶³ while on the D ring, the 20-hydroxyl and 21-carbonyl groups formed a hydrogen bond with THR739 and ASN⁵⁶⁴ of *hGRag* respectively. The 16 α formed 2 alkyl bonds to TYR735 and LEU732, while the 18 and 19-methyl groups displayed an alkyl interaction with, CYS736 and MET604 of *hGRag* respectively (Fig. 2a). A Pi-alkyl interaction was observed between the D ring and the remaining amino acid residues of *hGRag*. Glaucogenin C, the topmost ranked PDP for *hGRag* was also docked into the LBD of *hGRag*. The 3-hydroxyl and 15, 20 α -diepoxy groups of glaucogenin C interacted via hydrogen bonds with GLN⁵⁷⁰ and THR⁷³⁹, while the double bond between carbons 13 and 18 formed 2 hydrogen bonds with ASN⁵⁶⁴ and MET⁵⁶⁰. An alkyl interaction was observed between TRY⁷³⁵ and 19-methyl moiety, while several Pi-alkyl interactions were observed between the A, B and C rings and the remaining amino acid residues of *hGRag* (Fig. 2b). In a similar manner to

the 3'-carbonyl oxygen of dexamethasone, the 2-hydroxyl group of hirundigenin formed a hydrogen bond with ARG⁶¹¹, while the other hydrogen bond was formed between ASN⁵⁶⁴ of *hGRag* and 20-oxahexacyclo group. Numerous alkyl interactions were formed by 5- and 19-methyl groups while the pi-alkyl interactions were formed by the rings (Fig. 2c). Bregenin was also docked into the LBD of *hGRag*, interacting with the amino acid residues of the active site. The 3-, 16- and 17-hydroxyl groups of bregenin formed 3 hydrogen bonds with GLN⁵⁷⁰, GLN⁶⁴² and LEU⁷³² of *hGRag*. The 10- and 13-methyl groups formed alkyl interactions with MET⁶⁰¹, CYS⁷³⁶ and MET⁶⁰⁴ of *hGRag*. The remaining residues interacted via Pi-alkyl interaction with the B and C rings of bregenin (Fig. 2d). L(+)-tartaric acid, the reference inhibitor, and the native molecule bound to the crystallographic structure of *hIL-6* were docked into the “site 1” binding site. Five hydrogen bonds were observed between tartarate and IL-6. Direct hydrogen bonds to which ARG¹⁷⁹ and ARG¹⁸² of *hIL-6* served as the donors of four pairs of hydrogen atoms were formed with α -carboxyl moiety, while the α -hydroxyl group of the tartarate donated the hydrogen atom for the hydrogen bond with GLN¹⁷⁵ (Fig. 3a). ARG³⁰ and GLN¹⁷⁵ of *hIL-6* donated the hydrogen atoms for the hydrogen bonds formed with the carbonyl group of atratogenin A, while a carbon-hydrogen bond was formed between the furan ring and LEU³³(Fig. 3b). Alkyl interactions were formed between the 4 β -methyl moiety and ARG³⁰ and LEU³⁰ while Pi-alkyl interactions were formed by the B and furan rings with LEU¹⁷⁸ and LUE³³ of *hIL-6* respectively. Glaucogenin C was docked into the

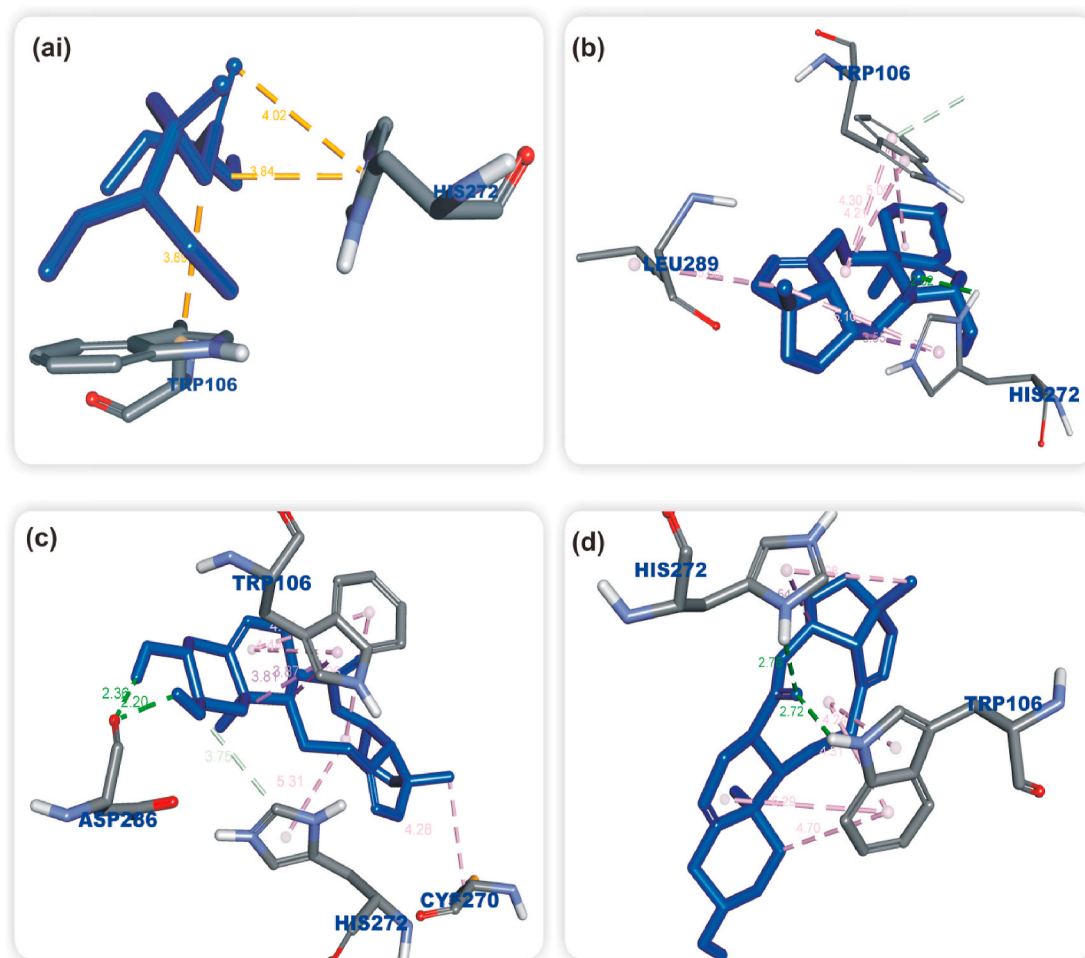


Fig. 6. Amino acid interactions of pregnanes in binding cavity of papain-like protease of SARS-CoV-2. Stick representations of ligands are coloured blue while interacting amino acids are in grey colour (a) Disulfiram (reference inhibitor) (b) glaucogenin D (c) glaucogenin A (d) glaucogenin C. Types of interactions are represented by green-dotted lines: H-bond interactions, light purple-dotted line: hydrophobic interactions (Pi-Alkyl, Alkyl & pi-stacking) purple-dotted line: Pi-Pi T Shaped, yellow-dotted lines: Pi-sulphur interactions, pi-stacking interactions. Three-letter amino acids are in black colour.

same binding site and interacted with some of the amino acid residues as methotrexate (Fig. 3c). A conventional hydrogen bond and carbon-hydrogen bond were formed with ARG¹⁸² and GLN¹⁷⁵ of hIL-6 respectively while most of the alkyl interactions were formed with 5- and 19-methyl groups. ASP³⁴ of hIL-6 donated a hydrogen atom to form hydrogen bond with 7-hydroxyl group, while the alkyl interactions were formed by the four rings of anhydroholantogenin (Fig. 3d). The amino group of the pyrimidine ring of roxolitinib (reference inhibitor) contributed two hydrogen atoms to form hydrogen bonds with GLU⁹⁵⁷ and GLY¹⁰²⁰ of hJAK1, while that of pyrazole ring formed two hydrogen bonds with ARG¹⁰⁰⁷ and ASN¹⁰⁰⁸ of hJAK1. Two Pi-sigma bonds were formed between the pyrrole ring of roxolitinib and LEU⁸⁸¹ and LEU¹⁰¹⁰. An alkyl interaction was observed between the cyclopentane ring of roxolitinib and ARG¹⁰⁰⁷ (Fig. 4a). The 6-hydroxyl group of atratogenin B donated the hydrogen atom for the only hydrogen bond formed with ARG¹⁰⁰³, while the 2- and 4-methyl groups and the methyl group attached to the furan ring interacted via alkyl interactions with VAL⁸⁸⁹, ALA⁹⁰⁶ and LEU¹⁰¹⁰ of hJAK1 respectively (Fig. 4b). Hirundigenin was docked into the same active site as roxolitinib; 8- and 16-hydroxyl groups and 20-oxahexacyclo ring of hirundigenin formed hydrogen bonds with LEU⁹⁵⁹ and ASN¹⁰⁰⁸, while the alkyl interactions were formed between the A and B rings and VAL⁸⁸⁹, LEU¹⁰¹⁰ and LEU⁸⁸¹ of hJAK1 (Fig. 4c). For glaucogenin C, the 21-carbonyl group formed two hydrogen bonds and the 8-hydroxyl group formed a hydrogen bond with ARG¹⁰⁰⁷, SER⁹⁶³ and GLY¹⁰²⁰ of hJAK1 respectively. The alkyl

interactions were majorly contributed by 5-methyl group of glaucogenin C (Fig. 4d). Ritonavir was docked into the receptor-binding site and interacted with amino acid residues that form the catalytic dyad (Cys-145 and His-41) of s3CL^{PRO} via a conventional hydrogen bond to LEU¹⁴¹ while the remaining interactions with HIS¹⁶⁴, THR²⁴ and CYS¹⁴⁵ were via carbon-hydrogen bonds. It further interacted via Pi-alkyl, Pi-Pi T-Shaped and Pi-sulphur with LEU²⁷, HIS⁴¹ and MET⁴⁹ of s3CL^{PRO} respectively (Fig. 5a). The three top ranked PDPs for s3CL^{PRO} were docked in the same binding site as the reference compound (ritonavir). Glaucogenin D interacted via conventional hydrogen and carbon-hydrogen bonds with GLY¹⁴³ and HIS⁴¹ of s3CL^{PRO}, while it interacted with MET¹⁶⁵ and THR²⁴ via alkyl interactions (Fig. 5b). A conventional hydrogen bond was formed between the 8- and 16-hydroxyl groups of hirundigenin and the catalytic residues (THR²⁴ and CYS¹⁴⁵) of s3CL^{PRO}, while the 19-methyl group formed an alkyl interaction with MET¹⁶⁵ (Fig. 5c). The 7-hydroxyl group of anhydroholantogenin formed hydrogen bond with THR²⁴ of s3CL^{PRO} while the remaining hydrophobic interactions were formed by 10- and 17-methyl groups and the rings (Fig. 5d). Disulfiram, a known inhibitor of PL^{PRO}, was docked into the binding cavity of SARS-COV-2 PL^{PRO}. It interacted with the amino acids HIS²⁷² and TRP¹⁰⁶ via a pi-sulphur interaction in the binding cavity of sPL^{PRO} (Fig. 6a). In the same vein, glaucogenin D, glaucogenin A and glaucogenin C were docked into the same binding site. The carbonyl and 19-methyl groups interacted via conventional hydrogen and Pi-alkyl interaction with HIS²⁷², while an alkyl interaction was observed with

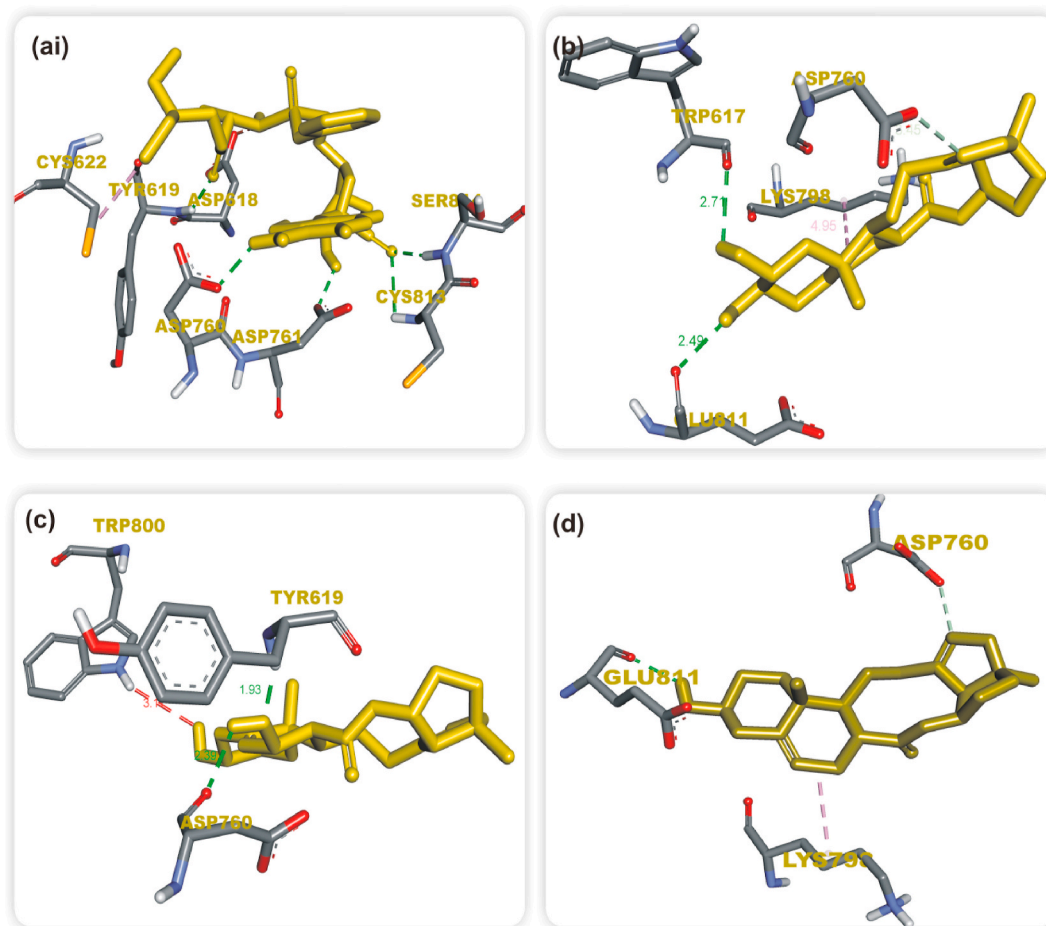


Fig. 7. Amino acid interactions of pregnanes in binding cavity of RNA-dependent RNA polymerase of SARS-CoV-2. Stick representations of ligands are coloured yellow while interacting amino acids are in grey colour (a) remdesivir (reference inhibitor) (b) glaucogenin A (c) glaucogenin D (c) glaucogenin C. Types of interactions are represented by green-dotted lines: H-bonds; light purple-dotted line: hydrophobic interactions (Pi-Alkyl, Alkyl & pi-stacking); purple-dotted line: Pi-Pi T Shaped; yellow-dotted lines: Pi-sulphur interactions, pi-stacking interactions. Three-letter abbreviations of amino acids are in black colour.

TRP¹⁰⁶ of sPL^{PRO} (Fig. 6b–d). The 7- and 8-hydroxyl groups of glaucogenin A formed two hydrogen bonds with ASP²⁸⁶, 8-hydroxyl group interacted via carbon-hydrogen bond with HIS²⁷², 19-methyl group interacted via alkyl interaction with CYS²⁷⁰, while the pentacyclo ring formed multiple Pi-Sigma bonds with TRP¹⁰⁶ (Fig. 6c). Two hydrogen bonds were formed between the carbonyl group of glaucogenin C and HIS²⁷² and TRP¹⁰⁶, while multiple Pi-alkyl interactions were formed with the same amino acid residues of sPL^{PRO} (Fig. 6d). The 4-aminopyrrolo[2,1-f] [1,2,4]triazin-7-yl, 5-cyno and carbonyl groups of sRdRp served as hydrogen donors for all of the conventional hydrogen bonds with the catalytic residues. The alkyl end of the 2-ethylbutyl moiety of sRdRp interacted via alkyl interaction with CYS⁶²², while an electrostatic force was formed between the phosphoryl group and APS⁶¹⁸ (Fig. 7a). In case of glaucogenin A, 7- and 8-hydroxyl groups of sRdRp formed two hydrogen bonds with GLU⁸¹¹ and TRP⁶¹⁷ respectively, while a conventional hydrogen bond and an alkyl interaction were formed by the double bonds at positions 21 and 10 with ASP⁷⁶⁰ and LYS⁷⁹⁸ respectively (Fig. 7b). The 12-hydroxyl group of Glaucogenin D formed the only two hydrogen bonds with APS⁷⁶⁰ and TRY⁶¹⁵ of sRdRp while Glaucogenin D exhibited similar binding pattern with that of Glaucogenin A (Fig. 7 c & d) (see Table 3).

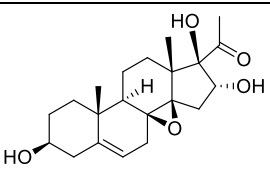
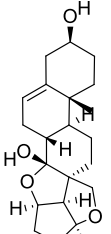
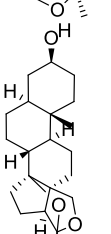
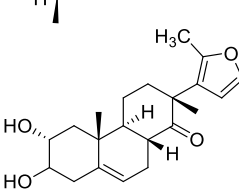
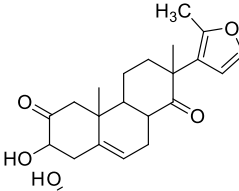
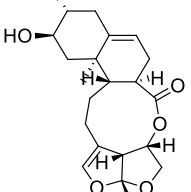
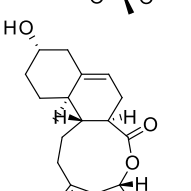
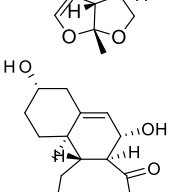
3.3. Results for molecular dynamics

The stability, structural/conformational fluctuations that occurred in the hGRag (apo protein), PDPs-hGRag and Dex-hGRag systems were

monitored in a simulated dynamic environment. The apo form and two complexes of hGRag with glaucogenin C and hirundigenin were used in a MDS study for 100 ns in NVT ensemble. The results were analyzed using VMD Tk console scripts to calculate RMSD, RMSF RoG, SASA, and H-bond.

The RMSD is a plausible measure of protein stability. The RMSD plots indicate how much each frame is deviated from the initial conformation of a reference structure as a function of time. The averages RMSD values of the apo protein (unbound), hGRag-glaucogenin C, hGRag-hirundigenin and hGRag-Dex complexes are 11.58 Å, 1.67 Å, 1.82 Å, and 1.68 Å, respectively (Fig. 8). The RMSF values give insights on the flexibility of amino acids with high values corresponding to high fluctuations. RMSF was calculated for C α atoms and the average values are 0.9 Å, 1.05 Å, 1.06 Å, 0.88 Å for the apo protein (unbound), hGRag-glaucogenin C, hGRag-hirundigenin and hGRag-Dex complexes respectively. The RMSF results show spikes at both the start and the end, which corresponds to the motion of the terminals. Few fluctuations were observed at amino acid residue number 27, 90, 180 and 243 in both the unbound and complexed hGRag proteins. Fig. 9 shows that residue: D21: D26, S89: N91, and Q104: R127 and R176: N183 have a larger fluctuation relative to the apo protein, this region are involved in the binding of the PDPs and Dex. The RoG plots gives information on the folding/unfolding properties while SASA plots indicate the surfaces exposed to solvent taking. Therefore, increasing values of SASA and RoG indicates that the protein have undergone unfolding. The averages of RoG and SASA are 18.67 Å and 14293 Å², for the apo protein (unbound); 18.75 Å and

Table 2Combined list of the top three ranked plant-derived pregnanes with the lowest binding energies for each of the protein targets in human and SARS-CoV 2^a.

S/No	Plant Pregnanes	Plant species
1	Bregenin 	<i>Sarcostemma brevistigma</i>
2	Hirundigenin 	<i>Vincetoxicum officinale</i>
3	Anhydroholantogenin 	<i>Holarrhena antidysenterica</i>
4	Atratogenin A 	<i>Cynanchum Atratum</i>
5	Atratogenin B 	<i>Cynanchum Atratum</i>
6	Glaucogenin A 	<i>Cynanchum glaucesens hand-maazz</i>
7	Glaucogenin C 	<i>Cynanchum glaucesens hand-maazz</i>
8	Glaucogenin D 	<i>Cynanchum glaucesens hand-maazz</i>

^a Protein Targets: Human glucocorticoid receptors in the agonist conformation (hGR α); human Interleukin-6 (hIL-6), human Janus kinases (hJAK1); SARS-CoV-2 3-chymotrypsin-like protease (s3CL^{Pro}); SARS-CoV-2 papain-like protease (sPL^{Pro}) and SARS-CoV-2 RNA-dependent RNA polymerase (sRdRp).

Table 3Interaction of reference inhibitors and plant derived pregnanes with amino acid residue of various targets^a.

Compounds	Protein	Numbers	Hydrogen bonds (Bond distance Å)	Numbers	Hydrophobic Interaction (Bond distance Å)	Numbers	Other interactions (Bond distance Å)
			Interacting residues		Interacting residues		Interacting residues
Dexamethasone	<i>hGRag</i>	2	ASN ⁵⁶⁴ (2.14) THR ⁷³⁹ (3.07) LEU ⁵⁶³ (3.07) ARG ⁶¹¹ (2.21)	8	TYR ⁷³⁵ (4.46) MET ⁶⁰¹ (5.44) LEU ⁷³² (4.68) CYS ⁷³⁶ (4.22) MET ⁶⁴⁶ (5.04) MET ⁶⁰⁴ (5.14)		none
Glucocogenin C		4	THR ⁷³⁹ (3.07) MET ⁵⁶⁰ (3.07) ASN ⁵⁶⁴ (3.07) GLN ⁵⁷⁰ (3.07)	7	TYR ⁷³⁵ (3.07) PHE ⁶²³ (3.07) LEU ⁷³² (3.07) LEU ⁶⁰⁸ (3.07) MET ⁶⁰¹ (3.07) MET ⁶⁴⁶ (3.07) LEU ⁵⁶³ (3.07)		none
Hirundigenin		2	ASN ⁵⁶⁴ (1.64) ARG ⁶¹¹ (3.17)	7	TYR ⁷³⁵ (5.30) PHE ⁶²³ (4.72) LEU ⁶⁰⁸ 5.41 MET ⁶⁰⁴ (5.23) MET ⁶⁴⁶ (5.33) LEU ⁵⁶³ (4.21) MET ⁶⁰¹ (5.23)		none
Bregenin		4	GLN ⁵⁷⁰ (2.03) GLN ⁶⁴² (2.24) LEU ⁷³² (2.57)	10	CYS ⁷³⁶ (3.71) PHE ⁶²³ (4.72, 4.81) LEU ⁶⁰⁸ 5.42 MET ⁶⁰⁴ (5.23, 5.20) MET ⁶⁴⁶ (5.35) LEU ⁵⁶³ (4.88, 3.73) MET ⁶⁰¹ (5.26)	2	LYS ³³⁶ (2) (4.08, 3.82)
Methotrexate	<i>hIL-6</i>	5	ARG ¹⁷⁹ (2.76, 3.04) ARG ¹⁸² (2.78, 2.74) GLN ¹⁷⁵ (2.80) GLN ¹⁷⁵ (2.01) ARG ³⁰ (2.79) LUE ³³ (3.68) LUE ¹⁷⁸ (2.89)	4	LUE ¹⁷⁸ (4.67) ARG ³⁰ (4.20) LUE ³³ (4.28, 4.87)		none
Atrategenin A		5	GLN ¹⁷⁵ (2.01) ARG ³⁰ (2.79) LUE ³³ (3.68) LUE ¹⁷⁸ (2.89)	4	ARG ³⁰ (3.92) LUE ³³ (4.05, 3.82) LUE ¹⁷⁸ (5.27) ARG ¹⁷⁹ (4.40)	2	none
Glucocogenin C		8	GLN ¹⁷⁵ (3.29) ARG ¹⁸² (2.44)	5	LUE ¹⁷⁸ (5.22, 4.50) ARG ¹⁷⁹ (5.49)		
Anhydroholantogenin		1	GLN ¹⁷⁵ (2.78)	3			
Ruxolitinib	<i>hJAK1</i>	4	ARG ¹⁰⁰⁷ (2.93) ASN ¹⁰⁰⁸ (2.16) GLU ⁹⁵⁷ (2.69) GLY ¹⁰²⁰ (2.23)	4	LEU ⁸⁸¹ (3.77) LEU ¹⁰¹⁰ (3.82) ALA ⁹⁰⁶ (4.80) ARG ¹⁰⁰⁷ (4.50)		
Atrategenin B		1	ARG ¹⁰⁰³ (2.85)	9	LEU ⁸⁸¹ (4.63, 4.63) LEU ¹⁰¹⁰ (3.46, 4.81, 4.81) ALA ⁹⁰⁶ (4.38) ARG ¹⁰⁰⁷ (4.50) VAL ⁸⁸⁹ (3.88, 5.15)		
Hirundigenin		3	ARG ¹⁰⁰⁷ (1.95, 3.77) LEU ⁹⁵⁹ (2.65) ASN ¹⁰⁰⁸ (2.37)	5	LEU ⁸⁸¹ (5.30, 4.09) LEU ¹⁰¹⁰ (3.46, 4.28) VAL ⁸⁸⁹ (4.38)		
Glucocogenin C		4	ARG ¹⁰⁰⁷ (3.02) SER ⁹⁶³ (2.81) GLY ⁸⁸² (3.66) GLY ¹⁰²⁰ (2.17)	5	LEU ⁸⁸¹ (5.36, 4.88) LEU ¹⁰¹⁰ (4.46) VAL ⁸⁸⁹ (4.32, 3.17)		
Ritonavir	<i>s3CL^{PRO}</i>	4	CYS ¹⁴⁵ (3.84) HIS ¹⁶⁴ (3.07) LEU ¹⁴¹ (2.88) THR ²⁴ (3.67)	3	LEU ²⁷ (5.41) HIS ⁴¹ (5.24) MET ⁴⁹ (4.82)		
Glucocogenin D		2	GLY ¹⁴³ (2.74) HIS ⁴¹ (3.36)	2	MET ¹⁶⁵ (5.07) THR ²⁴ (3.67)		
Hirundigenin		2	CYS ¹⁴⁵ (3.57) THR ²⁴ (2.50)	1	MET ¹⁶⁵ (4.26)		
Anhydroholantogenin		2	ASN ¹⁴² (3.67) THR ²⁴ (2.70)	7	CYS ¹⁴⁵ (5.47) HIS ⁴¹ (3.36, 5.36, 4.14) MET ⁴⁹ (4.43) MET ¹⁶⁵ (4.33, 5.46)		
Disulfiram	<i>sPL^{PRO}</i>			3	HIS ²⁷² (3.84, 4.01) TRP ¹⁰⁶ (1.06)		
Glucocogenin D		1	HIS ²⁷² (2.82)	5	TRP ¹⁰⁶ (4.21, 5.05, 4.30) HIS ²⁷² (3.54, 5.09)		
Glucocogenin A		3	HIS ²⁷² (3.75) ASP ²⁸⁶ (2.20, 2.35)	7	TRP ¹⁰⁶ (3.86, 3.81, 4.44, 4.60, 4.95) TRP ²⁷⁰ (4.27) HIS ²⁷² (5.31)		
Glucocogenin C		2	HIS ²⁷² (2.76) TRP ¹⁰⁶ (2.72)	6	HIS ²⁷² (3.54, 5.08) TRP ¹⁰⁶ (4.23, 5.28, 4.30, 4.70)		
Remdesivir	<i>sRdRp</i>	5	TYR ⁶¹⁹ (2.11) ASP ⁶¹ (2.72) CYS ⁸¹³ (2.79) SER ⁸¹⁴ (2.13) ASP ⁷⁶⁰ (2.17)	2	CYS ⁶²² (3.94) ASP ⁶¹³ (5.27)		
Glucocogenin A		3	GLU ⁸¹¹ (2.48) TRP ⁶¹⁷ (3.45) ASP ⁷⁶⁰ (2.17)	1	LYS ⁷⁹⁸ (4.95)		
Glucocogenin D		2	TRP ⁶¹⁹ (3.45) ASP ⁷⁶⁰ (2.17)		noon		
Glucocogenin C		2	GLU ⁸¹¹ (2.18) ASP ⁷⁶⁰ (3.36)	1	LYS ⁷⁹⁸ (3.98)		

^a Targets: Human glucocorticoid receptors in the agonist conformation (*hGRag*); human Interleukin-6 (*hIL-6*), human Janus kinases (*hJAK1*); SARS-CoV-2 3-chymotrypsin-like protease (*s3CL^{PRO}*); SARS-CoV-2 papain-like protease (*sPL^{PRO}*) and SARS-CoV-2 RNA-dependent RNA polymerase (*sRdRp*).

14,670 Å² for the *hGRag*-glucocogenin C; 18.82 Å and 14710 Å² for the *hGRag*-hirundigenin; and 18.64 Å and 14,353 Å² for the *hGRag*-Dex complexes respectively (Figs. 10 and 11). The average H-bonds for the apo protein (unbound), *hGRag*-glucocogenin C, *hGRag*-hirundigenin and *hGRag*-Dex complexes respectively are 69.33, 65.81, 68.42, and 67.2 respectively. The PDPs and Dex complexes had slightly lower number of hydrogen bonds than the unbound *hGRag* (Fig. 12). The binding free energy (ΔG_{bind}) measures the affinity of a ligand to its target protein. The free energy difference between the ligand-bound state (complex) and the corresponding unbound states of proteins and ligands are also employed in the calculations. Calculation of binding free energy ΔG_{bind} for *hGRag*-glucocogenin C, *hGRag*-hirundigenin and *hGRag*-Dex complexes using MM-GBSA implemented in Ambergtools 17 shows the binding free energies of -30.86 ± 2.8 kcal/mol, -35.22 ± 4.23 kcal/mol, and -39.83 ± 3.1 kcal/mol. The results of the binding free energy contribution per residue are shown in Fig. 13. Putting the three graphs in perspective, it was observed that in all the complexes, residue number

30–46, 71–81, around 120 and 201–210 corresponding to 558–574, 599–609, around 648 and 279–738 participated in the interactions to the PDPs and Dex. Table 4 shows the results of the number of clusters that were generated and the interactions at different clusters, using a representative conformer. The most common interactions in the *hGRag*-glucocogenin C and *hGRag*-hirundigenin complexes are hydrophobic with few hydrogen bonds. The *hGRag*-Dex complex indicated more hydrogen bonds. The most amino acid that commonly participates in the interactions of *hGRag*-glucocogenin C complex is LEU⁵⁶³ while in *hGRag*-hirundigenin complex there are two amino acids, which are LEU⁵⁶³ and LEU⁵⁶⁶. Figs. 13 and 14 show the first and last cluster of the *hGRag*-glucocogenin C complex while Figs. 15 and 16 show the first and last clusters of protein-hirundigenin complex. The amino acids that participated in interactions in *hGRag*-Dex complex are ASN⁵⁶⁴, GLN⁶⁴², and THR⁷³⁹ (see Fig. 16).

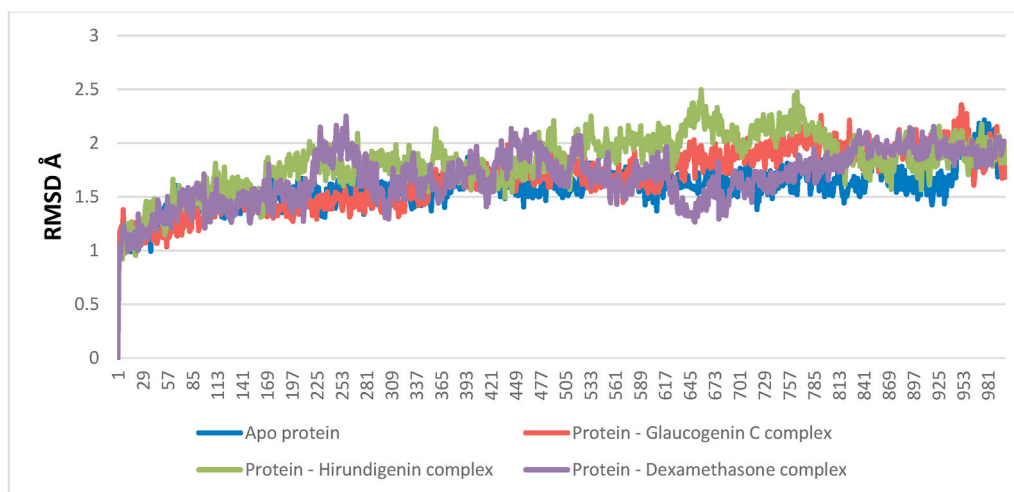


Fig. 8. Backbone-Root Mean Square Deviation plots of molecular dynamics (MD) simulation of *human* glucocorticoid receptors in the agonist conformation (hGRag), hGRag-hirundigenin, hGRag-glucocogenin and hGRag-dexamethasone complexes generated over 100 ns.

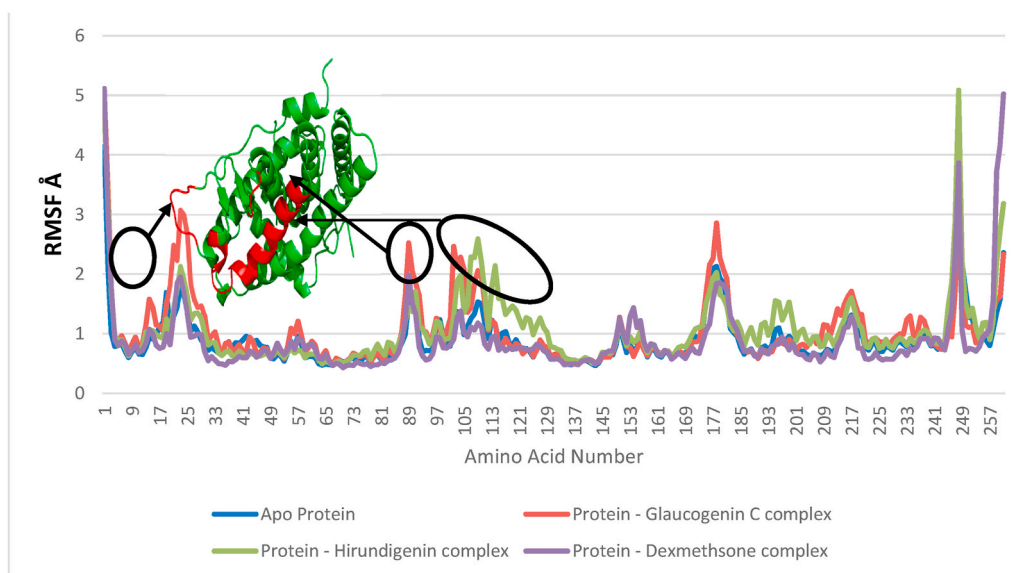


Fig. 9. Per residue Root Mean Square Fluctuations plots of molecular dynamics (MD) simulation of *human* glucocorticoid receptors in the agonist conformation (hGRag), hGRag-hirundigenin, hGRag-glucocogenin and hGRag-dexamethasone complexes generated over 100 ns.

3.4. Results for *in silico* drug-likeness and ADMET properties of top docked plant derived pregnanes to selected human and SARS-CoV-2 proteins

From the docking analysis, eight plant pregnanes (bregenin, hirundigenin, anhydroholantogenin, atratogenin A, atratogenin B, glaucogenin A, glaucogenin C and glaucogenin D) with high binding tendencies to hGRag with corresponding high binding tendencies to hIL-6, hJAK1, s3CL^{PRO}, sPL^{PRO}, and sRdRp were subjected to the predictive drug-likeness and ADMET (Absorption, Distribution, Metabolism, Excretion, and Toxicity) filtering analyses. The results for the predictive filtering analyses are presented in Table 5.

4. Discussion

Parallel advances in protein crystallography and various virtual-screening software for the modeling of ligand-receptor interactions have enhanced computer-aided drug design [49]. In this study a structure based virtual-screening of PDPs was employed via competitive

docking approach for hGR agonist with a dual inhibitory potential against cytokine storm syndrome and viral replication in COVID-19. The top potential agonists were further analyzed for multiplicity of inhibitory tendencies against the hIL-6 and hJAK1 (used as anti-proinflammatory targets), and s3CL^{PRO}, sPL^{PRO} and sRdRp (used as SARS-CoV-2 therapeutic targets). The docking of the PDPs to the hGRs identified the top ranked twenty PDPs with dexamethasone binding mode to hGR agonist. A total of eight PDPs were selected. From these eight PDPs, top three ranked PDPs (glaucogenin C, hirundigenin and bregenin) for hGR agonist were competitively and selectively docked to the hGRag. They were docked into the hydrophobic ligand binding pocket (LBP) which is located in the bottom half of the GR ligand binding domain, LBD [50,51]. The polar residues on the LBP interacted with the dexamethasone and the top ranked PDPs via several hydrogen bonds [51]. The binding of the amino acid residues on helix 12 and the loop preceding helix 12 have been earlier hypnotized to stabilize the helix in the active conformation that could serve as the molecular basis for the ligand-dependent activation of GR [52]. Among the several amino acids involved in the interactions, Cys-736 has been implicated in

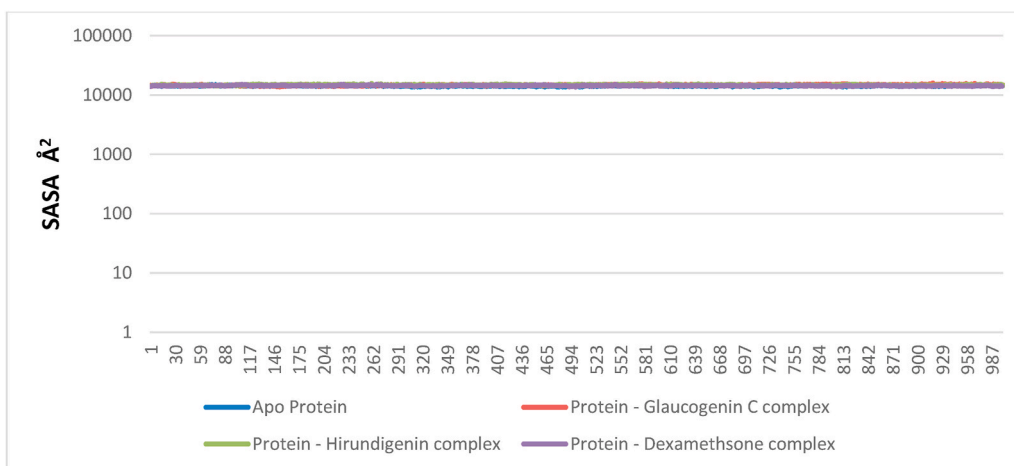


Fig. 10. Surface Accessible Surface Area plots of molecular dynamics (MD) simulation of *human* glucocorticoid receptors in the agonist conformation (hGRag), hGRag-hirundigenin, hGRag-glucocorticoid and hGRag-dexamethasone complexes generated over 100 ns.

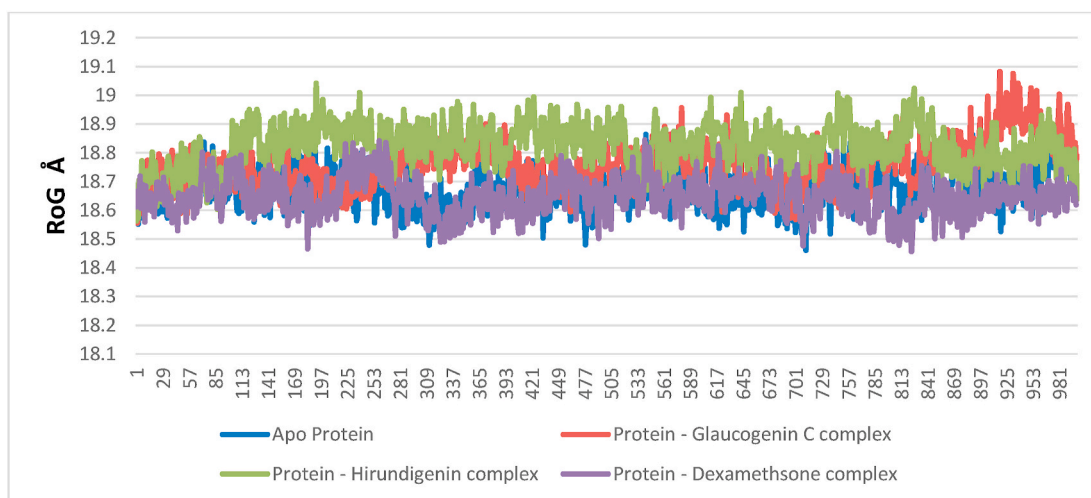


Fig. 11. Radius of gyration plots of molecular dynamics (MD) simulation of *human* glucocorticoid receptors in the agonist conformation (hGRag), hGRag-hirundigenin, hGRag-glucocorticoid and hGRag-dexamethasone complexes generated over 100 ns.

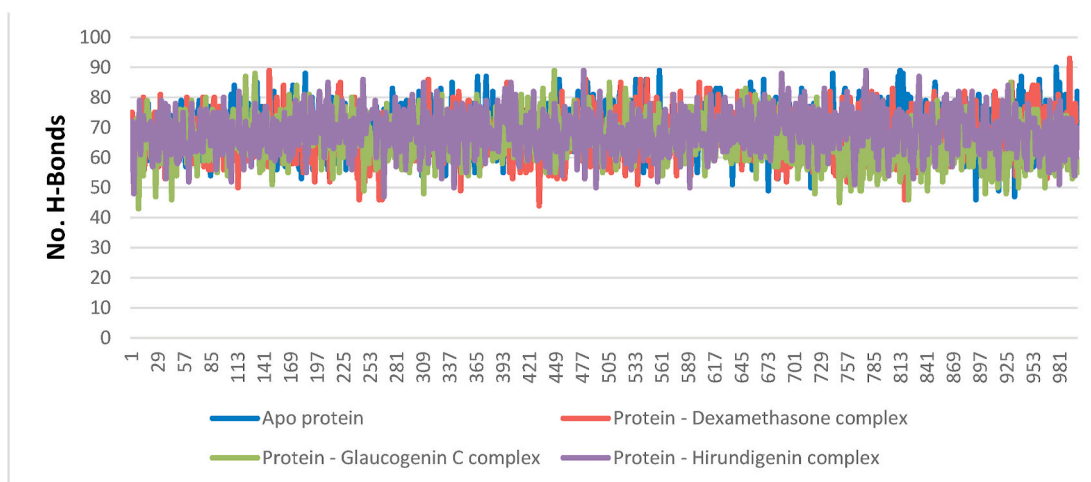


Fig. 12. Hydrogen bonds plots of molecular dynamics (MD) simulation of *human* glucocorticoid receptors in the agonist conformation (hGRag), hGRag-hirundigenin, hGRag-glucocorticoid and hGRag-dexamethasone complexes generated over 100 ns.

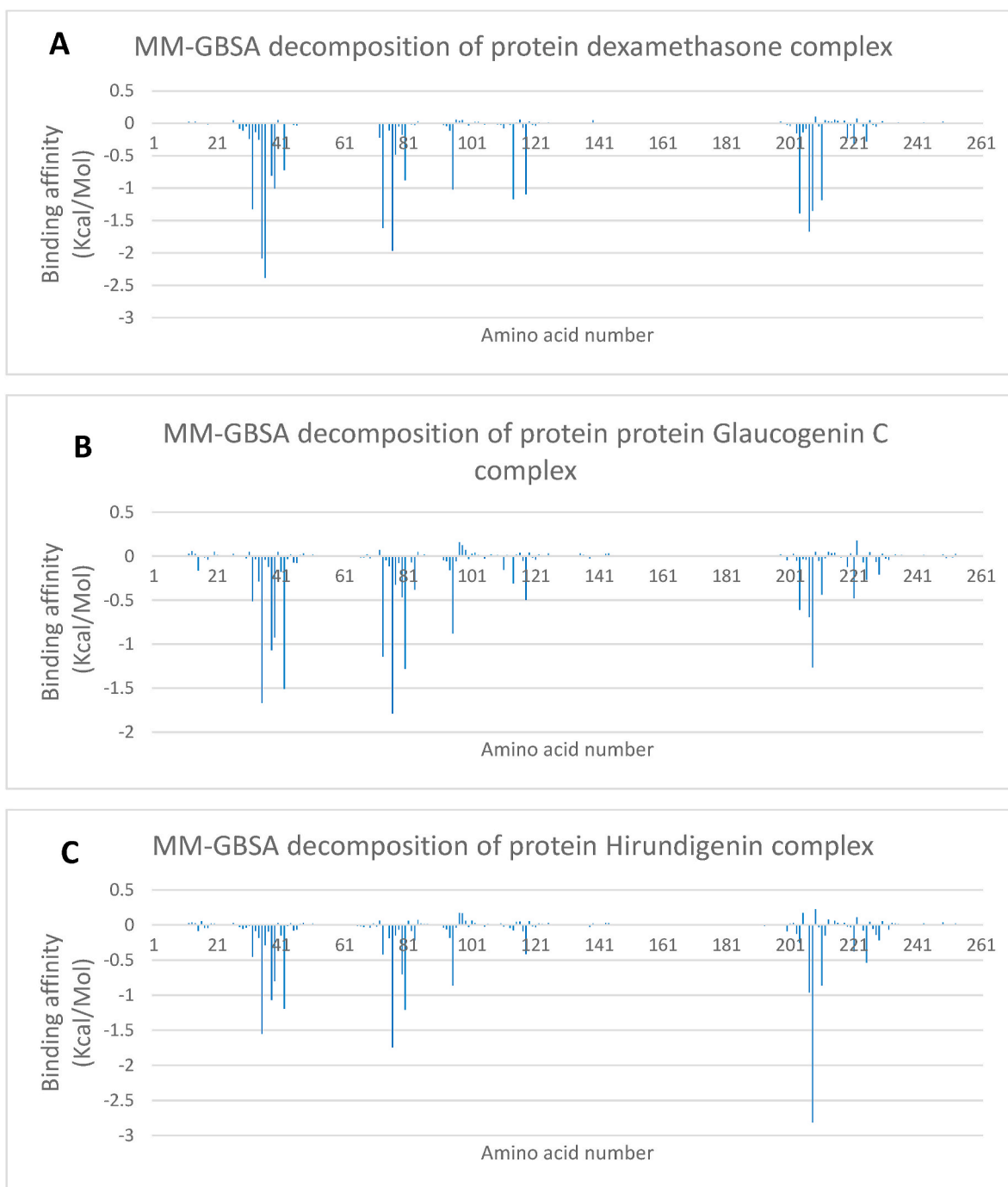


Fig. 13. Molecular mechanics/Poisson-Boltzmann surface area (MM/PBSA) plot of binding free energy contribution per residue of (A) hGRag-dexamethasone complex, (B) hGRag Glucocogenin C complex and (C) hGRag Hirundigenin complex.

the interactions with heat shock proteins [52], Tyr-735, has been shown to be important for transactivation [53], while Gln-642 have been reported to play a unique role in steroid recognition [52]. In addition to the steroid structures of glucocorticoids, the 3'-carbonyl oxygen, 2'-carbonyl oxygen, double bonds between C4 and C5, 17' hydroxyl group and 21' hydroxyl group, are critical for anti-inflammatory potency and glucocorticoid receptor affinity [54]. The identified PDPs contained similar and analogous functional groups that interacted with GR; thus, the binding of these plant steroidal pregnanes may initiate the ligand-dependent activation of GR since they share similar binding patterns with dexamethasone. The activated glucocorticoid-receptor complex can: (i) bind the promotor responsive elements (RE) of key

pro-inflammatory transcription factors (e.g. AP-1, NF kappa B) to inactivate them; (ii) upregulate the expression of cytokine inhibitory proteins, e.g. I kappa B, via glucocorticoid RE; and (iii) reduce the half-life time and usefulness of cytokine mRNAs [11]. IL-6 is a major causative factor of inflammatory disease and it is a promising target, as well as its signaling pathways; however, orally available small-molecule drugs specific for IL-6 have not been developed [55]. From the PDPs with high binding tendencies to hGRag, three PDPs (atratogeninA, glucocogenin C and anhydroholantogenin) exhibited the lowest binding energy poses for hIL-6 in the same binding site as observed for the co-crystallized ligands (tartaric acid) of hIL-6. In a similar study, furosemide exhibiting the same binding mode as tartaric acid was further

Table 4

The number of cluster, number and types of bonds for the human glucocorticoid receptors in the agonist conformation (hGRag) complexed to the top two-ranked PDPs and dexamethasone.

PROTEIN- COMPOUND COMPLEX	CLUSTER NUMBER	HYDROPHOBIC INTERACTIONS		H-BONDS	
		Number of interactions	Amino acids involved in the interaction	Number of interactions	Amino acids involved in the interaction
hGRag - glucocigenin C	Cluster 1	4	L563 L566 M604 L608	1	F623
	Cluster 2	3	W600 M604 L608	0	None
	Cluster 3	4	L563 (2) M604 L608	1	F623
	Cluster 4	4	L563 Q570 W600 T739	2	Q570 – Y735
	Cluster 5	7	L563 (2) L566 M604 L608 (2) Y735	2	N564 – Q570
hGRag -hirundigenin	Cluster 1	3	L563 L566 W600	0	None
	Cluster 2	5	L563 L566 M604 F740 F749	1	Q570
	Cluster 3	5	L563 L566 Q570 M604 I757	1	F623
	Cluster 4	5	L563 L566 Q570 T739 F749	1	F623
hGRag -Dexamethasone	Cluster 1	3	Q642 – L732 – Y735	5	N564 – Q642 (2)- T739 (2)
	Cluster 2	5	L566 – M604 – L608 – L732 – Y735	4	N564 (2) – Q642 – T739

The most common amino acids are in **bold**, amino acid residues are represented in one-letter format.

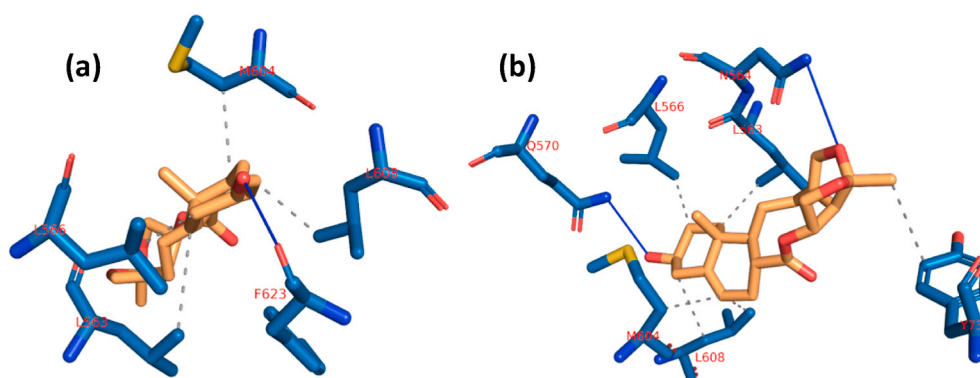


Fig. 14. Interactions in human glucocorticoid receptors in the agonist conformation (hGRag)-Glucocigenin C complex (a) cluster 1 and (b) cluster 5. Grey dotted dashed lines: hydrophobic interactions; Blue solid line: Hydrogen bond. Amino acids are in one-letter format and blue colour. Glucocigenin C is in orange stick representation.

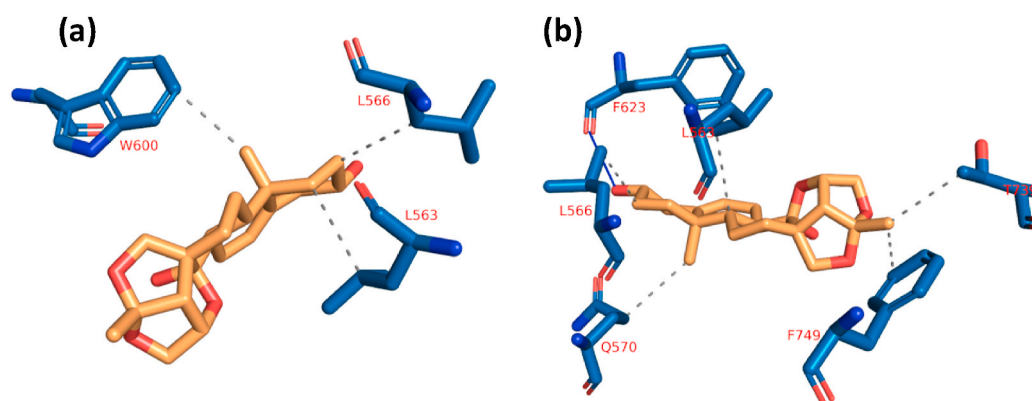


Fig. 15. Interactions in human glucocorticoid receptors in the agonist conformation (hGRag)-hirundigenin complex (a) cluster 1 and (b) cluster 4. Grey dotted dashed lines: hydrophobic interactions. Blue solid line: hydrogen-bond. Amino acids are in one-letter format and red colour. Hirundigenin is in orange stick representation.

found to inhibit hIL-6 activity *in vitro* [56]. From the X-ray crystal diffraction of hIL-6 structure, it was shown to contain four alpha helices (helices A, B, C, and D), which were linked with loops. The receptor-binding domain is located at the C-terminus (residues 175–181) [57], in which ARG¹⁷⁹ is known to be the key residue [57]. AB loop and helices A and D is important in receptor binding and signal transduction [58]. Compounds that interact strongly with residue ARG¹⁷⁹ may interfere with the binding of the receptor to its ligands [59],

thus these PDPs may proffer anti-inflammatory activity via hIL-6 inhibition. The Janus kinases (JAK) family of proteins function as critical mediators of cytokine signaling from membrane receptors to various signal transducers and activators of transcription (STAT) family of proteins [60]. Activation of STATs by the JAK kinases promotes the transcriptional activation of target genes controlling cell proliferation and survival, angiogenesis, and immune function [61]. Some JAK family inhibitors such as tofacitinib [62] and ruxolitinib [63] have progressed

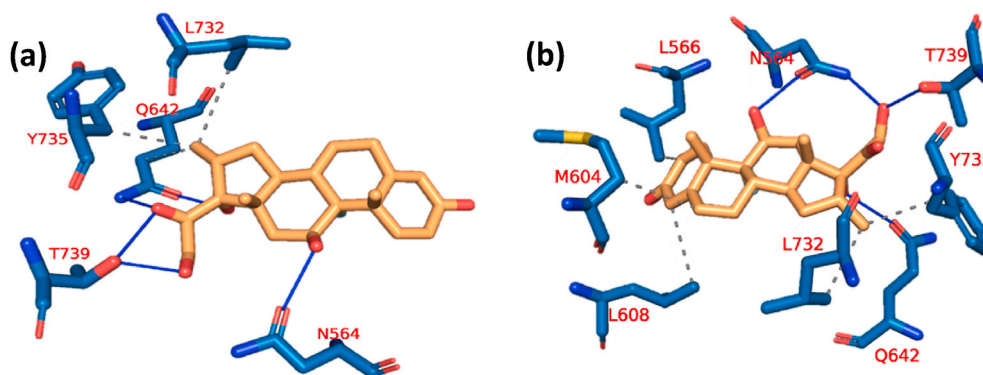


Fig. 16. Interactions in human glucocorticoid receptors in the agonist conformation (hGRag)–dexamethasone complex (a) cluster 1 and (b) cluster 2. Grey dotted dashed lines: hydrophobic interactions. Blue solid line: hydrogen-bond. Amino acids are in one-letter format and red colour. Dexamethasone is in orange stick representation.

into clinical trials, and FDA approvals. In comparison with the reference inhibitor, ruxolitinib, the top-three ranked PDPs (atratogenin B, hirundigenin, glaucogenin C) with the best binding modes, for which *h*JAK1 had the highest affinities, interacted with the hinge residues LEU⁹⁵⁹, GLU⁹⁵⁷ and the side chain of ASN¹⁰⁰⁸ and the backbone carbonyl oxygen of ARG¹⁰⁰⁷ of the catalytic residues. These residues are involved in the inhibitory activities of selected compounds in both *in silico* and *in vitro* analyses [64–66].

The catalytic dyad (His⁴¹ and Cys¹⁴⁵) of SARS-CoV-2 3CL^{pro} is domiciled between its domain I (residues 8–101) and domain II (residues 102–184) [67]. A long loop (residues 185–200) that connects domain II and domain III (residues 201–303) completes the 3CL^{pro} monomer [68]. The enzymatic activity of 3CL^{pro} resides in its catalytic dyad of Cys¹⁴⁵ and His⁴¹ [69]. The catalytic dyad and the residue Glu¹⁶⁶ have been reported to be involved in the protein dimerization and substrate cleaving through the catalytic activities present in the cleft between domains I and II. The substrate-binding pocket lies in the cleft consisting of residue 140–145 and 163, 166 of domain II [70,71]. The substrate-binding pocket is divided into a series of subsites (S1–S6), each accommodating a single but consecutive amino acid residue in the substrate. The key residues in the substrate binding pockets of 3CL^{pro} are His⁴¹, Tyr⁵⁴, Met⁴⁹, Phe¹⁴⁰-Cys¹⁴⁵, His¹⁶³–Pro¹⁶⁸, His¹⁷², and Asp¹⁸⁷–Gln¹⁹² regions [72]. In the same binding pattern as ritonavir (a known inhibitor of the protease), the top-three ranked pregnane (glaucogenin D, hirundigenin and anhydroholantogenin) were docked into the substrate binding pocket, interacting with various catalytic residues listed above. Considering our results and references to existing literature, the strong interaction of these PDPs to the critical residues (most especially HIS⁴¹, Gly¹⁴³, Cys¹⁴⁵ and MET¹⁶⁵) will greatly impair the dimerization and substrate binding of the SARS CoV-2 3CL^{pro}.

The catalytic triad of SARS-CoV-2 PL^{pro} is formed by CYS¹¹¹, HIS²⁷² and ASP²⁸⁶ [73,74], while TRP¹⁰⁶, GLY²⁵⁶, and LYS²⁷⁴ are catalytic residues (Li et al., 2020). LEU¹⁶², GLU¹⁶⁷, ASP¹⁶⁴ and TYR²⁶⁴ have been reported to be crucial for deubiquitinating activity of PL^{pro} [75]. The host innate immune system is critical to controlling SARS-CoV-2 infection. Reverse post-translational modifications of immune proteins, such as interferon factor 3 and NF- κ B via ubiquitination and the suppression of interferon-stimulated gene product 15 (ISG15), have also been implicated in the activities of PL^{pro} of SARS-CoV-2. [73,76], these, in turn, assist SARS-CoV-2 to escape the host innate immune responses. Pregnanes (glaucogenin D, hirundigenin and anhydroholantogenin) interacted with the catalytic triad and residues that are involved in deubiquitination. Such interactions may alter the catalytic conformation of PL^{pro} and inhibit its ability to reverse ubiquitination. SARS-CoV-2 RdRp plays a central role in coronaviral replication/transcription machinery; it is, therefore, accepted as an excellent target for new therapeutics for which lead inhibitors, such as remdesivir, have been

approved by the FDA [77]. Glaucogenin A, glaucogenin D and glaucogenin C were docked into the Motif C of the enzyme, exhibiting the same binding pattern as remdesivir. Motif C, the region comprising amino acid residues 753 to 767, contains the catalytic residues SER⁷⁵⁹, ASP⁷⁶⁰, and ASP⁷⁶¹ in the β -turn structure [77]. The stability of the complexes formed by the pregnanes with the enzyme stemmed from the vast number of interactions with the catalytic residues in the Motif C of the active site of the enzyme.

The several thermodynamics parameters (RMSD, RMSF, SASA and RoG) that were analyzed from the 100 ns full atomistic MDS trajectory files of the top two ranked PDPs-*h*GRag complexes revealed a high degree of stability throughout the period of the MDS run as compared to the apo receptor.

The RMSD plots showed that the binding of glaucogenin C and hirundigenin in the same manners as Dex to the active region of *h*GRag still preserved the structural integrity of the protein [78]. The

The RMSF plots indicates the flexibility of different regions of a protein and the amino acid residue along the trajectory, which can be related to crystallographic B factors [78]. The RMSF plots of the PDPs-*h*GRag complexes shows similar plot pattern with the Dex-*h*GRag complex. Though a lower amount of fluctuation occurred at with the interacting residues, it has been established that greater amounts of structural fluctuations usually occur in regions known to be involved in ligand binding and catalysis, notably the catalytic loop regions [79]. The RoG and SASA was assessed to evaluate the compactness and the accessibility of *h*GRag upon the binding of the PDPs and Dex. The PDPs and Dex maintained a reasonably steady RoG and SASA over the simulation time, indicating a highly compacted *h*GRag - PDPs and Dex complexes and well folded protein structure with intact intermolecular bonds [80]. The approximately close H-bonds between the top two ranked PDPs and Dex - *h*GRag complexes as compared to the unbound *h*GRag protein further indicated that the structural integrity of the protein was preserved in each of the system. At a quantitative level, simulation-based methods provide substantially more accurate estimates of ligand binding affinities (free energies) [81]. These results are calculated based on the total binding free energy of the complex. In these calculations, the binding free energy (ΔG_{bind}) measures the affinity of a ligand to its target protein. The free energy difference between the ligand-bound state (complex) and the corresponding unbound states of proteins and ligands are also employed in the calculations. Thus, the ΔG_{bind} calculations are important to gain in-depth knowledge about the binding modes of the hits in drug design [82]. The result from the MMPBSA calculation further corroborated the docking studies. Though Dex a known inhibitor to the *h*GRag protein presented the highest ΔG_{bind} , hirundigenin the top ranked PDP presented a very high and close ΔG_{bind} to Dex. A further evaluation of the MDS trajectories through clustering analysis showed that for each of the representative

Table 5*In silico* Physicochemical and ADMET^a parameters of plant derived pregnanes with lowest binding energies for selected human and SARS-CoV-2 proteins.

a) Physicochemical properties	Bregenin	Hirundigenin	Anhydroholantogenin	Atratogenin A	Atratogenin B	Glucogenin A	Glucogenin C	Glucogenin D
Molecular weight (g/mol)	364.48	362.46	332.26	344.44	342.433	376.44	360.44	376.44
Num. heavy atoms	26	26	24	25	25	27	26	27
Num. arom. Heavy atoms	0	0	0	5	5	0	0	0
Num. rotatable bonds	1	0	0	1	1	0	1	0
Num. H-bond acceptors	5	5	3	4	4	6	5	6
Hydrogen bond donor	4	2	1	2	1	2	1	2
cLogP	1.43	2.36	3.57	2.59	2.60	1.07	2.05	2.36
Molar Refractivity	98.53	95.04	93.26	96.08	95.11	97.10	95.94	97.10
TPSA (Å ²)	97.99	68.15	38.69	70.67	67.57	85.22	64.99	85.22
Drug-likeness								
Lipinski	Yes	Yes	Yes	Yes	Yes	Yes	Yes	Yes
Veber	Yes	Yes	Yes	Yes	Yes	Yes	Yes	Yes
Ghose	Yes	Yes	Yes	Yes	Yes	Yes	Yes	Yes
Egan	Yes	Yes	Yes	Yes	Yes	Yes	Yes	Yes
Muegge	Yes	Yes	Yes	Yes	Yes	Yes	Yes	Yes
Bioavailability Score	0.55	0.55	0.55	0.55	0.55	0.55	0.55	0.55
Absorption (Probability)								
(b) admet SAR								
Human Intestinal Absorption	HIA+ (0.659)	HIA+ (0.591)	HIA+ (0.729)	HIA+ (0.698)	HIA+ (0.758)	HIA+ (0.593)	HIA+ (0.689)	HIA+ (0.663)
Caco ⁻² Permeability Cm/s	Neg. (-5.32)	Neg. (-4.845)	Pos (-4.581)	Pos (-4.65)	Pos (-4.577)	Pos (-4.95)	Pos (-4.68)	Pos (-4.991)
P-glycoprotein Substrate	Neg. (0.061)	Neg. (0.089)	Neg. (0.103)	Neg. (0.045)	Neg. (0.043)	Neg. (0.086)	Neg. (0.039)	Neg. (0.037)
P-glycoprotein Inhibitor	Pos. (0.514)	Pos. (0.007)	Pos. (0.555)	Pos. (0.514)	Neg. (0.472)	Pos. (0.575)	Pos. (0.559)	Pos. (0.529)
Distribution (Probability)								
Blood-Brain Barrier	BBB+ (0.903)	BBB+ (0.657)	BBB+ (0.912)	BBB+ (0.932)	BBB+(0.956)	BBB+ (0.789)	BBB+ (0.855)	BBB+ (0.855)
PPB %	65.501	68.342	69.96	89.344	89.646	70.005	73.443	70.288
VD L/kg	0.147	0.106	0.296	0.406	0.197	-0.042	-0.058	-0.047
Metabolism (Probability)								
CYP450 1A2 Inhibitor	Neg. (0.044)	Neg. (0.050)	Neg. (0.043)	Neg. (0.037)	Neg. (0.04)	Neg. (0.09)	Neg. (0.083)	Neg. (0.066)
CYP450 1A2 Substrate	Neg. (0.381)	Neg. (0.306)	Neg. (0.252)	Neg. (0.382)	Neg. (0.384)	Neg. (0.384)	Neg. (0.36)	Neg. (0.356)
CYP450 3A4 Inhibitor	Neg. (0.047)	Neg. (0.113)	Neg. (0.134)	Neg. (0.105)	Neg. (0.144)	Neg. (0.189)	Neg. (0.174)	Neg. (0.189)
CYP450 3A4 Substrate	Neg. (0.716)	Pos. (0.658)	Pos. (0.516)	Pos. (0.71)	Pos. (0.57)	Pos. (0.459)	Pos. (0.691)	Pos. (0.638)
CYP4502C9 Inhibitor	Neg. (0.073)	Neg. (0.117)	Neg. (0.188)	Neg. (0.102)	Neg. (0.143)	Neg. (0.028)	Neg. (0.177)	Neg. (0.196)
CYP450 2C9 Substrate	Neg. (0.161)	Neg. (0.252)	Pos. (0.265)	Neg. (0.504)	Neg. (0.319)	Neg. (0.296)	Neg. (0.284)	Neg. (0.265)
CYP4502C19 Inhibitor	Neg. (0.138)	Neg. (0.142)	Neg. (0.24)	Neg. (0.253)	Neg. (0.222)	Neg. (0.144)	Neg. (0.139)	Neg. (0.144)
CYP450 2C19 Substrate	Neg. (0.400)	Pos. (0.588)	Pos. (0.178)	Pos. (0.563)	Pos. (0.551)	Pos. (0.536)	Pos. (0.544)	Pos. (0.572)
CYP4502D6 Inhibitor	Neg. (0.254)	Neg. (0.334)	Neg. (0.384)	Neg. (0.242)	Neg. (0.246)	Neg. (0.228)	Neg. (0.23)	Neg. (0.237)
CYP450 2D6 Substrate	Neg. (0.343)	Neg. (0.363)	Neg. (0.365)	Neg. (0.329)	Neg. (0.379)	Neg. (0.226)	Neg. (0.236)	Neg. (0.211)
Elimination								
T _{1/2} (Half Life Time)	1.453 h	1.408 h	1.822 h	1.673 h	1.555 h	1.221 h	1.302 h	1.364 h
CL (Clearance Rate) mL/min/kg	1.598	1.836	2.074	1.61	1.645	1.637	1.628	1.678
Toxicity								
hERG Blockers	Neg. (0.279)	Neg. (0.338)	Neg. (0.435)	Neg. (0.388)	Neg. (0.425)	Neg. (0.249)	Neg. (0.335)	Neg. (0.259)
H-HT	Neg. (0.622)	Neg. (0.488)	Neg. (0.294)	Pos. (0.77)	Pos. (0.592)	Pos. (0.73)	Neg. (0.762)	Neg. (0.68)
AMES (Ames Mutagenicity)	Neg. (0.174)	Neg. (0.242)	Neg. (0.218)	Neg. (0.092)	Neg. (0.74)	Neg. (0.26)	Neg. (0.26)	Neg. (0.36)
SkinSen (Skin sensitization)	Neg. (0.322)	Neg. (0.382)	Neg. (0.379)	Neg. (0.372)	Neg. (0.372)	Neg. (0.353)	Neg. (0.391)	Neg. (0.382)
LD ₅₀ of acute toxicity	3.32	3.356	2.986(343.02)	3.07(295.17)	3.065	3.263	3.177	3.362
In -log mol/kg (mg/kg)	(174.452)	(159.31)			(294.44)	(205.262)	(239.78)	(162.57)
DILI	Neg. 0.382	Neg. (0.254)	Neg. 0.412	Neg. 0.35	Neg. 0.204	Neg. 0.284	Neg. 0.332	Neg. (0.286)
Pharmacokinetics								
GI absorption	High	High	High	High	High	High	High	High
Log K _p (skin permeation) cm/s	-7.51	-7.41	-6.38	-6.54	-6.54	-7.84	-7.23	-7.92

^a ADMET: Absorption, distribution, metabolism, elimination, and toxicity; GI: Gastro-intestinal; BBB: Blood Brain Barrier; P-gp: permeability glycoprotein; CYP: cytochrome P450; hERG: human Ether-à-go-go-Related Gene; HIA: Human Intestinal Absorption; H-HT: Human Hepatotoxicity AMES: Ames Mutagenicity; DILI: Drug Induced Liver Injury; VD: Volume Distribution; PPB: Plasma Protein Binding.

conformers from the several clusters, the interactions (H-bonds and hydrophobic interaction) were preserved at different time frames, indicating that the interactions can be maintained in a dynamic environment, thus can be well adapted for experimental procedures.

Despite the various efforts to improve current glucocorticoids and anti-inflammatory drugs, they still pose significant side effects [83], Hence the top-docked PDPs to various proteins were subjected to *in silico* physicochemical and ADMET analysis. The eight top-ranked PDPs fulfilled the all the requirements for the five physicochemical filtering

analysis as reported by Lipinski [84] Ghose [85], Veber [86], Egan [87] and Muegge [88] thereby suggesting favourable physicochemical/druggable properties. The top-eight ranked PDPs expressed positive and high probability of human intestinal absorption and non-substrate but inhibitor of the permeability-glycoprotein (P-gp). These PDPs are predicted to be well absorbed into the blood stream subverting the capability of P-gp to pump them back into the intestinal lumen, bile ducts, urine-conducting ducts and capillaries respectively [89]. The blood brain barrier (BBB) penetration descriptor, predicts the ability of the

PDPs to penetrate the blood brain barrier. The top-eight PDPs displayed the properties that suggested their ability to cross the BBB. SARS-CoV-2 has been reported to infect the brain, thus indicating its ability to cross the BBB [90], these PDPs may cross the BBB for to exert an overall viral clearance.

The top-eight PDPs displayed a probability of at least 65% ability to be bound to the plasma protein, suggesting their ability to be transported by these proteins. The estimated half-life time (less than 2 h) and clearance ratefall within the moderate range. The three phytochemicals presented a tolerable LD₅₀ between (51–500 mg/kg). The hERG channel plays a vital role in the repolarization and termination stages of action potential in cardiac cells [91]. Compounds that block the hERG channel may cause cardiotoxicity [92]. The top-eight PDPs exhibit low probability of being a potential hERG channel blockers, suggesting that they may not cause hERG channel-related cardiotoxicity [92]. Using the mutagenicity and skin sensitization descriptors, the top-eight PDPs did not display the properties to be mutagenic *in silico*, thereby suggesting that they may not cause genetic mutations, which do initiate the pathophysiology of other diseases. The impact of the PDPs on the liver phase I drug metabolism was also analyzed using the various cytochrome P450 descriptors. The top-eight PDPs demonstrated no inhibitory potential for the various cytochrome P450, thus may not adversely affect phase I drug metabolism in the liver. ADME/tox analysis indicated high aqueous solubility, ability to pass the high human intestinal absorption, low acute oral toxicity with a good bioavailability score. Therefore this natural plant pregnane may be considered to be non toxic with drug-gable potential.

5. Conclusion

In this study we employed a competitive docking approach to screen 117 plant derived pregnanes (PDPs) for hGR agonist, with a dual inhibitory potential against SARS-CoV-2 infection and the accompanied cytokine storm syndrome. Eight PDPs (bregenin, hirundigenin, anhydroholantogenin, atratogenin A, atratogenin B, glaucogenin A, glaucogenin C and glaucogenin D) with high agonist binding tendencies to the hGRag displayed different levels of multiplicity of inhibitory potentials to other pro-inflammatory targets (hIL-6, hJAK1) and three SARS-CoV-2 therapeutic targets (s3CL^{pro}, sPL^{pro} and sRdRp). The 8 PDPs fulfilled the requirements for various physicochemical and ADMET descriptors thereby suggesting favourable druggable properties. The top two ranked PDPs (glaucogenin C and hirundigenin) complexed to the hGRag demonstrated a high degree of structural stability and flexibility in a 100 ns simulated dynamics environment. These promising hGRag agonists with anti-inflammatory and SARS-CoV-2 replication inhibitory potential is recommended for further *in vitro* and *in vivo* experiments.

Declaration of competing interest

The authors declare no conflicting interest.

Acknowledgements

The authors acknowledge with thanks resources offered by the PhytoBioNet platform. MDS calculations are done on the Bibliotheca Alexandrina HPC facility, Alexandria, Egypt.

Appendix A. Supplementary data

Supplementary data to this article can be found online at <https://doi.org/10.1016/j.compbiomed.2021.104406>.

Summary

The high morbidity and mortality rate of Severe Acute Respiratory Syndrome CoronaVirus 2 (SARS-CoV-2) infection arises majorly from

the Acute Respiratory Distress Syndrome (ARDS) and “cytokine storm” syndrome, which is sustained by an aberrant systemic inflammatory response and elevated pro-inflammatory cytokines. Thus, the identification of compounds which target multiple proteins in the virus and exhibit anti-inflammatory activity will enhance the development of effective drugs against the disease. In this study, we carried out an *in silico* evaluation of some plant-derived pregnanes for their activities against selected human pro-inflammatory and SARS-CoV-2 replication proteins targets. This was carried out by a virtual screening of an in-house library of steroidal plant-derived pregnanes (PDPs). One hundred and six (106) PDPs were docked into the active regions of *human* glucocorticoid receptors (hGRs) in the agonist (hGRag) and antagonist (hGRagt) conformation, in a competitive molecular docking approach. Based on the minimal binding energy and a comparative dexamethason binding mode analysis, a hit-list of the top twenty ranked PDPs that were docked in the agonist conformation of hGR, with binding energies ranging between –9.8 and –11.2 kcal/mol, was defined. The top twenty ranked PDPs were further analyzed for interactions with the *human* Janus kinases 1 and Interleukins-6 (hJAK1 and hIL-6 respectively), and SARS-CoV-2 3-chymotrypsin-like protease, Papain-like protease and RNA-dependent RNA polymerase (3CL^{pro}, PL^{pro} and RdRp respectively). For each of the 6 targeted proteins (3 humans and 3 SARS CoV-2), the top three ranked PDPs were selected, to give a sum of eight PDPs (bregenin, hirundigenin, anhydroholantogenin, atratogenin A, atratogenin B, glaucogenin A, glaucogenin C and glaucogenin D) with multiplicity of high binding tendencies to the catalytic residues of different targets. From this eight PDPs, glaucogenin C and hirundigenin having the highest agonist tendencies to the hGR were further subjected to a 100 ns atomistic molecular dynamics simulation. A high degree of structural stability was observed from molecular dynamics simulation analyses of glaucogenin C and hirundigenin complexes of hGRag. A further clustering of the MDS trajectories of the complexes of glaucogenin C and hirundigenin with the hGRag shows that the interactions of these PDPs with the active site residues of hGRag were preserved in different representative structures of the clusters. The selected top-eight ranked PDPs demonstrated favourable druggable properties over the Lipinski, Veber, Ghose, Egan and Muegge predictive filters. In the same vein the 8 PDPs displayed favourable *in silico* ADMET properties over a wide range of predictive molecular descriptors, such as, ability to pass the blood brain barriers, high intestinal absorption, non-substrate to the permeability glycoprotein, non hERG blockers, non inhibitors of the cytochrome p450 etc. Thus, these promising hGRag agonists, especially glaucogenin C and hirundigenin, with potential anti-inflammatory and SARS-CoV-2 replication inhibitory activity is recommended for lead optimization for drug candidate and further evaluation in an *in vitro* and *in vivo* experiment.

Funding

The research did not receive any funding or grants.

Ethical

Approval: Not applicable.

Consent to participate

Not applicable.

Consent to publish

Not applicable.

Authors contributions

G. A. Gyebi Conceived and designed the analysis.

O. M. Ogunyemi Performed molecular docking analysis.
 I. M. Ibrahim Performed molecular simulations.
 J. O. Adebayo Editing and review of manuscript
 S. O. Afolabi Editing and review of manuscript.

Availability of data and materials

The authors confirm that the data supporting the findings of this study are available within the article [and/or] its supplementary materials.

References

- C. Huang, Y. Wang, X. Li, L. Ren, J. Zhao, Y. Hu, L. Zhang, G. Fan, J. Xu, X. Gu, Clinical features of patients infected with 2019 novel coronavirus in Wuhan, China, *Lancet* 395 (2020) 497–506.
- C.I. Paules, H.D. Marston, A.S. Fauci, Coronavirus infections—more than just the common cold, *Jama* 323 (2020) 707–708.
- F. Coperchini, L. Chiovato, L. Croce, F. Magri, M. Rotondi, The Cytokine Storm in COVID-19: an Overview of the Involvement of the Chemokine/chemokine-Receptor System, *Cytokine & Growth Factor Reviews*, 2020.
- K. Ratia, K.S. Saikatendu, B.D. Santarsiero, N. Barretto, S.C. Baker, R.C. Stevens, A. D. Mesecar, Severe acute respiratory syndrome coronavirus papain-like protease: structure of a viral deubiquitinating enzyme, *Proc. Natl. Acad. Sci. Unit. States Am.* 103 (2006) 5717–5722.
- J.M. Ferrara, S. Abhyankar, D. Gilliland, Cytokine Storm of Graft-Versus-Host Disease: a Critical Effector Role for Interleukin-1, *Transplantation proceedings*, 1993, pp. 1216–1217.
- K. Yuen, S. Wong, Human infection by avian influenza A H5N1, *Hong Kong Med. J.* 11 (3) (2005) 189–199.
- M.Z. Tay, C.M. Poh, L. Rénia, P.A. MacAry, L.F.P. Ng, The trinity of COVID-19: immunity, inflammation and intervention, *Nat. Rev. Immunol.* 20 (2020) 363–374.
- C. Huang, Y. Wang, X. Li, L. Ren, J. Zhao, Y. Hu, L. Zhang, G. Fan, J. Xu, X. Gu, Z. Cheng, T. Yu, J. Xia, Y. Wei, W. Wu, X. Xie, W. Yin, H. Li, M. Liu, Y. Xiao, H. Gao, L. Guo, J. Xie, G. Wang, R. Jiang, Z. Gao, Q. Jin, J. Wang, B. Cao, Clinical features of patients infected with 2019 novel coronavirus in Wuhan, China, *Lancet* 395 (2020) 497–506.
- M. Soy, G. Keser, P. Atagunduz, F. Tabak, I. Atagündüz, S. Kayhan, Cytokine storm in COVID-19: pathogenesis and overview of anti-inflammatory agents used in treatment, *Clin. Rheumatol.* 39 (2020).
- C.C. Chow, S.S. Simons Jr., An approach to greater specificity for glucocorticoids, *Front. Endocrinol.* 9 (2018) 76.
- R. Brattsand, M. Linden, Cytokine modulation by glucocorticoids: mechanisms and actions in cellular studies, *Aliment. Pharmacol. Ther.* 10 (1996) 81–90.
- V. Sannarangappa, R. Jalleh, Inhaled corticosteroids and secondary adrenal insufficiency, *Open Respir. Med. J.* 8 (2014) 93.
- P. Poletto, G. Alvarez-Rivera, T.M. Torres, J.A. Mendiola, E. Ibañez, A. Cifuentes, Compressed fluids and phytochemical profiling tools to obtain and characterize antiviral and anti-inflammatory compounds from natural sources, *Trac. Trends Anal. Chem.* (2020) 115942.
- A. Gosslau, S. Li, C.T. Ho, K.Y. Chen, N.E. Rawson, The importance of natural product characterization in studies of their anti-inflammatory activity, *Mol. Nutr. Food Res.* 55 (2011) 74–82.
- K. Ghoreschi, A. Laurence, J.J. O’Shea, Janus kinases in immune cell signaling, *Immunol. Rev.* 228 (2009) 273–287.
- C. Schindler, D.E. Levy, T. Decker, JAK-STAT signaling: from interferons to cytokines, *J. Biol. Chem.* 282 (2007) 20059–20063.
- C. Ding, G. Jones, Anti-interleukin-6 receptor antibody treatment in inflammatory autoimmune diseases, *Rev. Recent Clin. Trials* 1 (2006) 193–200.
- A. Zumla, J.F. Chan, E.I. Azhar, D.S. Hui, K.Y. Yuen, Coronaviruses - drug discovery and therapeutic options, *Nature reviews, Drug discovery* 15 (2016) 327–347.
- L. Kiemer, O. Lund, S. Brunak, N. Blom, Coronavirus 3CL pro proteinase cleavage sites: possible relevance to SARS virus pathology, *BMC Bioinf.* 5 (2004) 72.
- G.A. Gyebi, O.B. Ogunro, A.P. Adegunloye, O.M. Ogunyemi, S.O. Afolabi, Potential inhibitors of coronavirus 3-chymotrypsin-like protease (3CLpro): an in silico screening of alkaloids and terpenoids from African medicinal plants, *J. Biomol. Struct. Dyn.* (2020) 1–19.
- G.A. Gyebi, A.P. Adegunloye, I.M. Ibrahim, O.M. Ogunyemi, S.O. Afolabi, O. B. Ogunro, Prevention of SARS-CoV-2 cell entry: insight from in silico interaction of drug-like alkaloids with spike glycoprotein, human ACE2, and TMPRSS2, *J. Biomol. Struct. Dyn.* (2020) 1–25.
- O.M. Ogunyemi, G.A. Gyebi, A.A. Elfiky, S.O. Afolabi, O.B. Ogunro, A. P. Adegunloye, I.M. Ibrahim, Alkaloids and flavonoids from African phytochemicals as potential inhibitors of SARS-Cov-2 RNA-dependent RNA polymerase: an in silico perspective, *Antiviral Chem. Chemother.* 28 (2020), 2040206620984076.
- D.W. Cain, J.A. Cidlowski, After 62 years of regulating immunity, dexamethasone meets COVID-19, *Nat. Rev. Immunol.* 20 (2020) 587–588.
- S.K. Patel, G. Saikumar, J. Rana, J. Dhama, M.I. Yatoo, R. Tiwari, A.J. Rodríguez-Morales, G. Dhama, Dexamethasone: a boon for critically ill COVID-19 patients? *Trav. Med. Infect. Dis.* 37 (2020), 101844.
- Q.-C. Huang, M.-J. Wang, X.-M. Chen, W.-L. Yu, Y.-L. Chu, X.-H. He, R.-Y. Huang, Can active components of licorice, glycyrrhizin and glycyrrhetic acid, lick rheumatoid arthritis? *Oncotarget* 7 (2016) 1193.
- R. Shah, V. Gulati, E.A. Palombo, Pharmacological properties of guggulsterones, the major active components of gum guggul, *Phytother Res.* 26 (2012) 1594–1605.
- S. Darshan, R. Doreswamy, Patented antiinflammatory plant drug development from traditional medicine, *Phytother Res.: An International Journal Devoted to Pharmacological and Toxicological Evaluation of Natural Product Derivatives* 18 (2004) 343–357.
- S. Bale, G. Pulivendala, C. Godugu, Withaferin A attenuates bleomycin-induced scleroderma by targeting FoxO3a and NF- κ B signaling: connecting fibrosis and inflammation, *Biofactors* 44 (2018) 507–517.
- A. Haratake, D. Watase, S. Setoguchi, N. Nagata-Akaho, K. Matsunaga, J. Takata, Effect of orally ingested diosgenin into diet on skin collagen content in a low collagen skin mouse model and its mechanism of action, *Life Sci.* 174 (2017) 77–82.
- N. Panda, S. Banerjee, N.B. Mandal, N.P. Sahu, Pregnane glycosides, *Natural Product Communications* 1 (2006), 1934578X0600100813.
- G.A. Gyebi, J.O. Adebayo, O.E. Olorundare, A. Pardeed, M. Ninomiya, A.O. Saheed, A.S. Babatunde, M. Koketsu, Iloneoside: a cytotoxic ditigloylated pregnane glycoside from the leaves of *Gongronema latifolium* Benth, *Nat. Prod. Res.* 32 (2018) 2882–2886.
- Z.-m. Lin, Y.-t. Liu, Y.-t. Huang, X.-q. Yang, F.-h. Zhu, W. Tang, W.-m. Zhao, S.-j. He, J.-p. Zuo, Anti-nociceptive, anti-inflammatory and anti-arthritic activities of pregnane glycosides from the root bark of *Periploca sepium* Bunge, *J. Ethnopharmacol.* 265 (2021) 113345.
- J. Min, L. Perera, J.M. Krahn, C.M. Jewell, A.F. Moon, J.A. Cidlowski, L. C. Pedersen, Probing dominant negative behavior of glucocorticoid receptor β through a hybrid structural and biochemical approach, *Mol. Cell Biol.* 38 (2018).
- H.W. Ng, W. Zhang, M. Shu, H. Luo, W. Ge, R. Perkins, W. Tong, H. Hong, Competitive molecular docking approach for predicting estrogen receptor subtype α agonists and antagonists, *BMC bioinformatics, BioMed Central* (2014) S4.
- S. Dallakyan, A.J. Olson, Small-molecule Library Screening by Docking with PyRx, *Springer*, 2015, pp. 243–250. *Chemical biology*.
- O. Trott, A.J. Olson, AutoDock Vina, Improving the speed and accuracy of docking with a new scoring function, efficient optimization, and multithreading, *J. Comput. Chem.* 31 (2010) 455–461.
- N.M. O’Boyle, M. Banck, C.A. James, C. Morley, T. Vandermeersch, G. R. Hutchison, Open label: an open chemical toolbox, *J. Cheminf.* 3 (2011), 33-33.
- J.C. Phillips, R. Braun, W. Wang, J. Gumbart, E. Tajkhorshid, E. Villa, C. Chipot, R. D. Skeel, L. Kale, K.J. Schulten, Scalable molecular dynamics with NAMD, *J. Comput. Chem.* 26 (2005) 1781–1802.
- B.R. Brooks, C.L. Brooks III, A.D. Mackerell Jr., L. Nilsson, R.J. Petrella, B. Roux, Y. Won, G. Archontis, C. Bartels, S.J. Boresch, CHARMM: the biomolecular simulation program, *J. Comput. Chem.* 30 (2009) 1545–1614.
- J. Lee, X. Cheng, J.M. Swails, M.S. Yeom, P.K. Eastman, J.A. Lemkul, S. Wei, J. Buckner, J.C. Jeong, Y.J. Qi, computation, CHARMM-GUI input generator for NAMD, GROMACS, AMBER, OpenMM, and CHARMM/OpenMM simulations using the CHARMM36 additive force field 12 (2016) 405–413.
- W. Humphrey, A. Dalke, K.J. Schulten, VMD: visual molecular dynamics 14 (1996) 33–38.
- C.-M. Suomivuori, N.R. Latorraca, L.M. Wingler, S. Eismann, M.C. King, A. L. Kleinhenz, M.A. Skiba, D.P. Staus, A.C. Kruse, R.J. Lefkowitz, Molecular mechanism of biased signaling in a prototypical G protein-coupled receptor, *Science* 367 (2020) 881–887.
- B.R. Miller III, T.D. McGee Jr., J.M. Swails, N. Homeyer, H. Gohlke, A.E. Roitberg, MMPBSA.py: an efficient program for end-state free energy calculations, *J. Chem. Theor. Comput.* 8 (2012) 3314–3321.
- T. Tubiana, J.-C. Carvillat, Y. Boulard, S.p.J. Bressanelli, modeling, TTClust: a versatile molecular simulation trajectory clustering program with graphical summaries 58 (2018) 2178–2182.
- S. Salentin, S. Schreiber, V.J. Haupt, M.F. Adasme, M.J.N.a.r. Schroeder, PLIP: fully automated protein–ligand interaction profiler 43 (2015) W443–W447.
- W.L. DeLano, PyMOL (2002).
- A. Daina, O. Michielin, V. Zoete, SwissADME: a free web tool to evaluate pharmacokinetics, drug-likeness and medicinal chemistry friendliness of small molecules, *Sci. Rep.* 7 (2017) 42717.
- F. Cheng, W. Li, Y. Zhou, J. Shen, Z. Wu, G. Liu, P.W. Lee, Y. Tang, admetSAR: a comprehensive source and free tool for assessment of chemical ADMET properties, *J. Chem. Inf. Model.* 52 (2012) 3099–3105.
- W. Yu, A.D. MacKerell, *Computer-aided Drug Design Methods*, Springer, *Antibiotics*, 2017, pp. 85–106.
- L.D. Álvarez, M.A. Martí, A.S. Veleiro, D.M. Presman, D.A. Estrin, A. Pecci, G. Burton, Exploring the molecular basis of action of the passive antiluciferase 21-hydroxy-6, 19-epoxyprogesterone, *J. Med. Chem.* 51 (2008) 1352–1360.
- L.D. Álvarez, M.A. Martí, A.S. Veleiro, R.I. Misico, D.A. Estrin, A. Pecci, G. Burton, Hemisuccinate of 21-hydroxy-6, 19-epoxyprogesterone: a tissue-specific modulator of the glucocorticoid receptor, *ChemMedChem: Chemistry Enabling Drug Discovery* 3 (2008) 1869–1877.
- B. Kauppi, C. Jakob, M. Färnegårdh, J. Yang, H. Ahola, M. Alarcon, K. Calles, O. Engström, J. Harlan, S. Muchmore, The three-dimensional structures of antagonistic and agonistic forms of the glucocorticoid receptor ligand-binding domain ru-486 induces a transconformation that leads to active antagonism, *J. Biol. Chem.* 278 (2003) 22748–22754.

- [53] D. Ray, C.-S. Suen, A. Brass, J. Soden, A. White, Structure/function of the human glucocorticoid receptor: tyrosine 735 is important for transactivation, *Mol. Endocrinol.* 13 (1999) 1855–1863.
- [54] M. Katz, E.H. Gans, Topical corticosteroids, structure-activity and the glucocorticoid receptor: discovery and development—a process of “planned serendipity”, *J. Pharmaceut. Sci.* 97 (2008) 2936–2947.
- [55] S.-S. Hong, J.H. Choi, S.Y. Lee, Y.-H. Park, K.-Y. Park, J.Y. Lee, J. Kim, V. Gajulapati, J.-I. Goo, S. Singh, A novel small-molecule inhibitor targeting the IL-6 receptor β subunit, glycoprotein 130, *J. Immunol.* 195 (2015) 237–245.
- [56] Z. Wang, Y. Wang, P. Vilekar, S.-P. Yang, M. Gupta, M.I. Oh, A. Meek, L. Doyle, L. Villar, A. Brennecke, Small molecule therapeutics for COVID-19: repurposing of inhaled furosemide, *PeerJ* 8 (2020), e9533.
- [57] R. Somers, M. Stahl, J.S. Seehra, 1.9 Å crystal structure of interleukin 6: implications for a novel mode of receptor dimerization and signaling, *EMBO J.* 16 (1997) 989–997.
- [58] R. Savino, A. Lahm, A.L. Salvati, L. Ciapponi, E. Sporeno, S. Altamura, G. Paonessa, C. Toniatti, G. Ciliberto, Generation of interleukin-6 receptor antagonists by molecular-modeling guided mutagenesis of residues important for gp130 activation, *EMBO J.* 13 (1994) 1357–1367.
- [59] M. Ehlers, J. Grötzinger, M. Fischer, H.K. Bos, J.P. Brakenhoff, S. Rose-John, Identification of single amino acid residues of human IL-6 involved in receptor binding and signal initiation, *J. Interferon Cytokine Res.* 16 (1996) 569–576.
- [60] K. Yamaoka, P. Saharinen, M. Pesu, V.E. Holt, O. Silvennoinen, J.J. O’Shea, The janus kinases (jaks), *Genome Biol.* 5 (2004) 1–6.
- [61] W. Vainchenker, S.N. Constantinescu, JAK/STAT signaling in hematological malignancies, *Oncogene* 32 (2013) 2601–2613.
- [62] C. Rakeh, P.G. Conaghan, Tofacitinib for treatment of rheumatoid arthritis, *Adv. Ther.* 30 (2013) 713–726.
- [63] M.M. Vasbinder, M. Alimzhanov, M. Augustin, G. Bebernitz, K. Bell, C. Chuaqui, T. Deegan, A.D. Ferguson, K. Goodwin, D. Huszar, Identification of azabenzimidazoles as potent JAK1 selective inhibitors, *Bioorg. Med. Chem. Lett* 26 (2016) 60–67.
- [64] M.L. Vazquez, N. Kaila, J.W. Strohbach, J.D. Trzuppek, M.F. Brown, M.E. Flanagan, M.J. Mitton-Fry, T.A. Johnson, R.E. TenBrink, E.P. Arnold, Identification of N-(cis-3-[Methyl (7 H-pyrrolo [2, 3-d] pyrimidin-4-yl) amino] cyclobutyl) propane-1-sulfonamide (PF-04965842): a selective JAK1 clinical candidate for the treatment of autoimmune diseases, *J. Med. Chem.* 61 (2018) 1130–1152.
- [65] Q. Su, E. Banks, G. Bebernitz, K. Bell, C.F. Borenstein, H. Chen, C.E. Chuaqui, N. Deng, A.D. Ferguson, S. Kawatkar, Discovery of (2 R)-N-[3-[2-[(3-Methoxy-1-methyl-pyrazol-4-yl) amino] pyrimidin-4-yl]-1 H-indol-7-yl]-2-(4-methylpiperazin-1-yl) propanamide (AZD4205) as a potent and selective janus kinase 1 inhibitor, *J. Med. Chem.* 63 (2020) 4517–4527.
- [66] M. Zak, E.J. Hanan, P. Lupardus, D.G. Brown, C. Robinson, M. Siu, J.P. Lyssikatos, F.A. Romero, G. Zhao, T. Kellar, Discovery of a class of highly potent Janus kinase 1/2 (JAK1/2) inhibitors demonstrating effective cell-based blockade of IL-13 signaling, *Bioorg. Med. Chem. Lett* 29 (2019) 1522–1531.
- [67] L. Zhang, D. Lin, X. Sun, U. Curth, C. Drosten, L. Sauerhering, S. Becker, K. Rox, R. Hilgenfeld, Crystal structure of SARS-CoV-2 main protease provides a basis for design of improved α -ketoamide inhibitors, *Science* 368 (2020) 409–412.
- [68] H. Yang, W. Xie, X. Xue, K. Yang, J. Ma, W. Liang, Q. Zhao, Z. Zhou, D. Pei, J. Ziebuhr, Design of wide-spectrum inhibitors targeting coronavirus main proteases, *PLoS Biol.* 3 (2005) e324.
- [69] H. Yang, M. Yang, Y. Ding, Y. Liu, Z. Lou, Z. Zhou, L. Sun, L. Mo, S. Ye, H. Pang, G. F. Gao, K. Anand, M. Bartlam, R. Hilgenfeld, Z. Rao, The crystal structures of severe acute respiratory syndrome virus main protease and its complex with an inhibitor, *Proc. Natl. Acad. Sci. U. S. A.* 100 (2003) 13190–13195.
- [70] H.L. Nguyen, N.Q. Thai, D.T. Truong, M.S. Li, Remdesivir strongly binds to both RNA-dependent RNA polymerase and main protease of SARS-CoV-2: evidence from molecular simulations, *J. Phys. Chem. B* 124 (50) (2020) 11337–11348.
- [71] S. Vardhan, S.K. Sahoo, In silico ADMET and molecular docking study on searching potential inhibitors from limonoids and triterpenoids for COVID-19, *Comput. Biol. Med.* 124 (2020) 103936.
- [72] Z. Jin, X. Du, Y. Xu, Y. Deng, M. Liu, Y. Zhao, B. Zhang, X. Li, L. Zhang, C. Peng, Structure of M pro from SARS-CoV-2 and discovery of its inhibitors, *Nature* 582 (2020) 289–293.
- [73] B.T. Freitas, I.A. Durie, J. Murray, J.E. Longo, H.C. Miller, D. Crich, R.J. Hogan, R. A. Tripp, S.D. Pegan, Characterization and noncovalent inhibition of the deubiquitinase and deISGylase activity of SARS-CoV-2 papain-like protease, *ACS Infect. Dis.* 6 (8) (2020) 2099–2109.
- [74] Q. Li, W. Peng, Y. Ou, Prediction and analysis of key protein structures of 2019-nCoV, *Future Virol.* 15 (6) (2020).
- [75] C.-Y. Chou, H.-Y. Lai, H.-Y. Chen, S.-C. Cheng, K.-W. Cheng, Y.-W. Chou, Structural basis for catalysis and ubiquitin recognition by the severe acute respiratory syndrome coronavirus papain-like protease, *Acta Crystallogr. Sect. D Biol. Crystallogr.* 70 (2014) 572–581.
- [76] C.M. Daczkowski, J.V. Dzimiński, J.R. Clasman, O. Goodwin, A.D. Mesecar, S. D. Pegan, Structural insights into the interaction of coronavirus papain-like proteases and interferon-stimulated gene product 15 from different species, *J. Mol. Biol.* 429 (2017) 1661–1683.
- [77] Y. Gao, L. Yan, Y. Huang, F. Liu, Y. Zhao, L. Cao, T. Wang, Q. Sun, Z. Ming, L. Zhang, Structure of the RNA-dependent RNA polymerase from COVID-19 virus, *Science* 368 (2020) 779–782.
- [78] X. Cheng, I. Ivanov, *Molecular dynamics, Computational toxicology* (2012) 243–285.
- [79] Y.-w. Dong, M.-I. Liao, X.-I. Meng, G.N. Somero, Structural flexibility and protein adaptation to temperature: molecular dynamics analysis of malate dehydrogenases of marine molluscs, *Proc. Natl. Acad. Sci. Unit. States Am.* 115 (2018) 1274–1279.
- [80] S. Sinha, S.M. Wang, Classification of VUS and unclassified variants in BRCA1 BRCT repeats by molecular dynamics simulation, *Comput. Struct. Biotechnol. J.* 18 (2020) 723–736.
- [81] A. Perez, J.A. Morrone, C. Simmerling, K.A. Dill, Advances in free-energy-based simulations of protein folding and ligand binding, *Curr. Opin. Struct. Biol.* 36 (2016) 25–31.
- [82] P.A. Kollman, I. Massova, C. Reyes, B. Kuhn, S. Huo, L. Chong, M. Lee, T. Lee, Y. Duan, W. Wang, Calculating structures and free energies of complex molecules: combining molecular mechanics and continuum models, *Acc. Chem. Res.* 33 (2000) 889–897.
- [83] H. Schäcke, W.-D. Döcke, K. Asadullah, Mechanisms involved in the side effects of glucocorticoids, *Pharmacol. Ther.* 96 (2002) 23–43.
- [84] C.A. Lipinski, Avoiding investment in doomed drugs, *Curr. Drug Discov.* 1 (2001) 17–19.
- [85] A.K. Ghose, V.N. Viswanadhan, J.J. Wendoloski, A knowledge-based approach in designing combinatorial or medicinal chemistry libraries for drug discovery. I. A qualitative and quantitative characterization of known drug databases, *J. Comb. Chem.* 1 (1999) 55–68.
- [86] D.F. Veber, S.R. Johnson, H.-Y. Cheng, B.R. Smith, K.W. Ward, K.D. Kopple, Molecular properties that influence the oral bioavailability of drug candidates, *J. Med. Chem.* 45 (2002) 2615–2623.
- [87] W.J. Egan, K.M. Merz, J.J. Baldwin, Prediction of drug absorption using multivariate statistics, *J. Med. Chem.* 43 (2000) 3867–3877.
- [88] I. Muegge, S.L. Heald, D. Brittelli, Simple selection criteria for drug-like chemical matter, *J. Med. Chem.* 44 (2001) 1841–1846.
- [89] J.H. Lin, M. Yamazaki, Role of P-glycoprotein in pharmacokinetics, *Clin. Pharmacokinet.* 42 (2003) 59–98.
- [90] L. Zanin, G. Saraceno, P.P. Panciani, G. Renisi, L. Signorini, K. Migliorati, M. Fontanella, SARS-CoV-2 can induce brain and spine demyelinating lesions, *Acta Neurochir.* (2020) 1–4.
- [91] E. Raschi, V. Vasina, E. Poluzzi, F. De Ponti, The hERG K⁺ channel: target and antitarget strategies in drug development, *Pharmacol. Res.* 57 (2008) 181–195.
- [92] J.M. Kratz, U. Grienke, O. Scheel, S.A. Mann, J.M. Rollinger, Natural products modulating the hERG channel: heartaches and hope, *Nat. Prod. Rep.* 34 (2017) 957–980.

Dr. Gideon A. Gyebi is currently a lecturer at the Department of Biochemistry, Faculty of Science and Technology Bingham University, Karu, Nasarawa, Nigeria. He obtained his Ph.D in Biochemistry in cancer chemoprevention and toxicology from the Department of Biochemistry, University of Ilorin, Kwara state, Nigeria. He was a former faculty member of the College of Natural and Applied Sciences, Salem University, Nigeria. He was a visiting researcher to the Department of Chemistry and Biomolecular Sciences, Faculty of Engineering, and the Anaerobic Research Unit of Gifu University, (1-1 Yanagido Gifu) Japan. His research interests are natural product Chemistry, Bioinformatics malaria and cancer chemotherapy. He is a pioneer of the PhytoBioNet: Phytochemistry and Bioinformatic Network.

Ogunyemi Oludare Michael currently works as a lecturer in the Department of Biochemistry, Salem university Nigeria. He has received several research awards which include the African-German Network of Excellence in Sciences (AGNES). He was a visiting researcher to the Food security and safety research niche, Northwest University, Mafikeng, South Africa. His current research interest is Human Nutraceuticals and Bioinformatics.

Ibrahim Mohamed Ibrahim is a master degree candidate in Department of Biophysics, Cairo University, Egypt. He is a researcher in Dr. Abdo A. Elfiky research group. He has published several papers related to structural bioinformatics.

Professor Joseph O. Adebayo is currently a professor of clinical biochemistry and biochemical toxicology at the Department of Biochemistry, Faculty of Life Sciences, University of Ilorin, Nigeria. He obtained his Ph.D in Biochemistry (Clinical option) from the University of Ilorin, Kwara state, Nigeria. He is a former postdoctoral fellow at the Instituto René Rachou, FIOCRUZ, Belo Horizonte MG, Brasil. His research interests are malaria chemotherapy and diagnosis. He has presented various academic as well as research-based papers at several national and international conferences including Society of Toxicology USA. He has supervised several Ph.D students, one of such is Dr. Gideon A. Gyebi.

Dr. Saheed O. Afolabi is currently a lecturer at the Department of Pharmacology and Therapeutics, Faculty of Basic Medical Sciences, University of Ilorin, Ilorin, Nigeria. He obtained his Ph.D in Ethnopharmacology with focus on cancer chemo prevention and toxicology from the Department of Pharmacology and Therapeutics, Faculty of Basic Medical Sciences University of Ilorin, Ilorin, Nigeria. He was a visiting researcher to the Department of Chemistry and Biomolecular Sciences, Faculty of Engineering, and the Anaerobic Research Unit of Gifu University, (1-1 Yanagido Gifu) Japan, and Department of Dermatology, University of Wisconsin, Madison, WI 53706, USA.